TU WIEN Informatics

Gestaltung einer visuellen Analyse-Pipeline zur Untersuchung der TMS-Wirkungen auf die Herzfrequenz

DIPLOMARBEIT

zur Erlangung des akademischen Grades

Diplom-Ingenieurin

im Rahmen des Studiums

Medizinische Informatik

eingereicht von

Ráchel Grexová, BSc
Matrikelnummer 01605767

an der Fakultät für Informatik

der Technischen Universität Wien

Betreuung: Associate Prof. Dr.in Renata Georgia Raidou

Wien, 1. September 2025

Ráchel Grexová	Renata Georgia Raidou

Technische Universität Wien
A-1040 Wien ▪ Karlsplatz 13 ▪ Tel. +43-1-58801-0 ▪ www.tuwien.at

TU WIEN Informatics

Designing a Visual Analysis Pipeline for Exploring TMS Effects on Heart Rate

DIPLOMA THESIS

submitted in partial fulfillment of the requirements for the degree of

Diplom-Ingenieurin

in

Medical Informatics

by

Ráchel Grexová, BSc
Registration Number 01605767

to the Faculty of Informatics

at the TU Wien

Advisor: Associate Prof. Dr.in Renata Georgia Raidou

Vienna, September 1, 2025

Ráchel Grexová	Renata Georgia Raidou

Technische Universität Wien
A-1040 Wien ▪ Karlsplatz 13 ▪ Tel. +43-1-58801-0 ▪ www.tuwien.at

Erklärung zur Verfassung der Arbeit

Ráchel Grexová, BSc

Hiermit erkläre ich, dass ich diese Arbeit selbständig verfasst habe, dass ich die verwendeten Quellen und Hilfsmittel vollständig angegeben habe und dass ich die Stellen der Arbeit – einschließlich Tabellen, Karten und Abbildungen –, die anderen Werken oder dem Internet im Wortlaut oder dem Sinn nach entnommen sind, auf jeden Fall unter Angabe der Quelle als Entlehnung kenntlich gemacht habe.
Ich erkläre weiters, dass ich mich generativer KI-Tools lediglich als Hilfsmittel bedient habe und in der vorliegenden Arbeit mein gestalterischer Einfluss überwiegt. Im Anhang „Übersicht verwendeter Hilfsmittel“ habe ich alle generativen KI-Tools gelistet, die verwendet wurden, und angegeben, wo und wie sie verwendet wurden. Für Textpassagen, die ohne substantielle Änderungen übernommen wurden, haben ich jeweils die von mir formulierten Eingaben (Prompts) und die verwendete IT- Anwendung mit ihrem Produktnamen und Versionsnummer/Datum angegeben.

Wien, 1. September 2025

Ráchel Grexová

Acknowledgements

Throughout the design, implementation, and writing of this thesis, I have received a great deal of support and assistance. I would like to thank my advisor, Associate Prof. Dr.in Renata Georgia Raidou, for invaluable support, advice, and guiding me through this Master's thesis. I would like to thank Martin Tik, Ph.D., and the fMRI lab from the Medical University of Vienna for the measured data that we used in the thesis. In addition, I would like to thank my parents for their general support during the writing of this Master's thesis.

Kurzfassung

Wir haben eine hochflexible, visuelle Analyse-Pipeline in Jupiter Notebooks entwickelt, um die transkranielle Magnetstimulation (TMS) und die Herzfrequenz (HF) in verschiedenen kognitiven Zuständen von Probanden zu untersuchen. TMS ist eine vielversprechende Behandlungsmethode für schwere depressive Störungen, die nicht auf pharmakologische Behandlungen ansprechen. Der Wirkmechanismus ist jedoch noch nicht vollständig aufgeklärt. Die Forschung zu den besten Erfassungseinstellungen, wie Stimulationsintensitäten und Zielorte, befindet sich noch im Anfangsstadium. Eine multimodale Analysepipeline, die TMS, funktionelle Magnetresonanztomographie (fMRI) und HF integriert, könnte Aufschluss über die Nervenbahnen geben und die Effizienz der TMS steigern. Um die bereits verfügbare Pipeline zur simultanen TMS-fMRI-Analyse auf die multimodale gleichzeitige TMS-fMRI-HR-Analyse auszuweiten, ist die Untersuchung der Auswirkungen der TMS auf die HR der nächste Schritt. Um die Pipeline für visuelle Analyse zu gestalten, führen wir eine Erweiterung des Daten-Nutzer-Aufgaben Designdreiecks [Miksch and Aigner, 2014] ein und wenden diese an, indem wir den bisherigen Workflow-Ansatz in den Gestaltungsprozess integrieren. Da sich der Datenverarbeitungs-Workflow in diesem Bereich noch in der Entwicklung befindet, bietet die Integration des bisherigen Workflow-Ansatzes in den Designprozess Vorteile, indem das Datenerbe respektiert, die Anpassungsfähigkeit der Benutzer unterstützt und die Kompatibilität der Aufgaben sichergestellt wird. Wir bezeichnen dieses Framework als Daten-Benutzer-Workflow-Aufgaben Designpyramide. Anschließend stellen wir eine visuelle Analyse-Pipeline bereit, um die Datenexploration in den frühen Phasen der Forschung zu unterstützen. Die interaktive Vorverarbeitungs-Pipeline umfasst die Extraktion von Daten, die Behandlung fehlender Daten und die Rauschunterdrückung. Um Zeitreihen der HR mit unterschiedlichen Eigenschaften zu vergleichen, visualisieren wir die Ähnlichkeitsmessung Dynamic Time Warping (DTW) und das Clustering der Herzfrequenzvariabilität (HFV). Wir bewerten die Vorverarbeitungsschritte quantitativ anhand simulierter EKG-Daten. Das wichtigste Ergebnis ist, dass lineare und polynomiale Interpolation mit RMSE-Werten (Root Mean Squared Error) von nur -3 bzw. -5-te Potenze als Imputationsmethoden für EKG mit einer Abtastfrequenz von 400 Hz besonders effektiv sind. Zur Bewertung des Nutzungsszenarios für die TMS- und EKG-Datenexploration, verwenden wir die Qualitative Inspektion der Ergebnisse (QRI). Unsere vorgeschlagene visuelle Analyse-pipeline stellt die ersten Schritte zur Integration der TMS-HR-Analyse in einen trimodalen simultanen TMS-fMRI-HF-Ansatz dar.

Abstract

We designed a highly flexible notebook-based visual analysis pipeline to explore Transcranial Magnetic Stimulation (TMS) and heart rate (HR) in different subjects' cognitive states. TMS is a promising treatment of major depressive disorder not responsive to pharmacological treatment. However, the mechanism of action is not yet fully understood. The research in the best acquiring settings, such as stimulation intensities and target sites, is emerging. Multimodal analysis pipeline integrating TMS, Functional Magnetic Resonance Imaging (fMRI), and HR could shed light on both understanding the neural pathways and increasing the efficiency of TMS. To extend the already available concurrent TMS-fMRI analysis pipeline towards multimodal concurrent TMS-fMRI-HR, exploring the effect of TMS on HR is the next step. To design the visual analysis pipeline, we introduce and apply an extension of Data–Users–Tasks design triangle [Miksch and Aigner, 2014] by integrating the previous data workflow approach in the designing process. When the data processing workflow in the domain is only evolving, integrating the previous workflow approach into the design process benefits by respecting the data legacy, supports users' adaptability, and ensures tasks' compatibility. We refer to this framework as the Data–Users–Workflow-Tasks design pyramid. We subsequently provide a visual analysis pipeline to support data exploration in the early stages of research. The interactive preprocessing pipeline involves extracting data, handling missing data, and reducing noise. To compare time series of HR with different properties, we visualize Dynamic Time Warping (DTW) similarity measurement, and heart rate variability (HRV) metric clustering. We quantitatively evaluate the preprocessing steps using simulated ECG data. The key result is that linear and polynomial interpolation with root mean squared error (RMSE) values as low as to the power of -3 and -5, respectively, are especially effective as imputation methods for ECG with 400 Hz sampling frequency. To further assess the values of the usage scenarios for TMS and ECG data exploration, we employ Qualitative Result Inspection (QRI). Our proposed visual analysis pipeline assembles the first steps towards integrating TMS-HR analysis into a trimodal concurrent TMS-fMRI-HR approach.

Contents

CHAPTER 1

Introduction

1.1 Motivation

Treatment of mental health problems such as major depressive disorder (MDD) remains a challenge, as about 30% of the patients do not respond to pharmacological treatment [Chen et al., 2023]. This condition is called treatment-resistant depression (TRD) [Chen et al., 2023]. In the United States, the Food and Drug Administration (FDA) has approved 10 Hz repetitive TMS (rTMS) targeting dorsolateral prefrontal cortex (DLPFC) for TRD and other psychiatric disorders [O'Reardon et al., 2007]. In real-world studies, 50% to 80% patients with TRD respond to modern accelerated rTMS protocol treatment [Chen et al., 2023].

However, the neural mechanism of action of Transcranial Magnetic Stimulation (TMS) is not yet fully understood [Tik et al., 2023a]. To study neural activation responses during stimulation, concurrent TMS-fMRI is used. This approach requires that TMS and Functional Magnetic Resonance Imaging (fMRI) are acquired simultaneously [Mizutani-Tiebel et al., 2022]. Furthermore, major depressive disorder is linked with heart rate changes, including increased risk of heart disease [Iseger et al., 2021]. Some studies have shown that TMS decreases heart rate [Makovac et al., 2017; Rossi et al., 2016; Udupa et al., 2007]. Neuro-Cardiac-Guided Transcranial Magnetic Stimulation (NCG-TMS) studies the effects of TMS on HR [Iseger et al., 2017].

Although TMS is an approved treatment for TRD by the FDA, clinical applications lack evidence-based methods that allow researchers to determine the most suitable stimulation intensities at a target site and taking into account the inter-subject variability [Tik et al., 2023a]. The combination of TMS with fMRI [Grosshagauer et al., 2024] or ECG [Iseger et al., 2021] can be used to estimate the effective target site and intensity of TMS. Furthermore, TMS-fMRI allows to study the short- and long-term neural response to TMS [Tik et al., 2023b] and NCG-TMS studies the effects of TMS on HR and is easier to apply in clinical practice [Dijkstra et al., 2023].

Integrating the three modalities into one approach could enhance the benefits of both concurrent TMS-fMRI and NCG-TMS. Yet, there is a gap between neuroimaging research and clinical psychiatric applications, as studies often focus on binary differential outcome at the group level. To support the process of diagnosis, prognosis, and treatment of psychiatric disorders, individualized approaches would be beneficial [Ward et al., 2021]. Multimodal analysis of TMS, fMRI, and ECG could provide more information on correlations within the bimodal approaches and their results. Linking effects of TMS-modulation on fMRI and ECG is anticipated to provide an individualized approach to integrate neuroimaging research into clinical practice, as ECG can also be measured in clinical practice [Dijkstra et al., 2023].

To find the best possible solutions, the data acquisition protocols and data processing pipelines are evolving, and a pipeline for processing ECG and TMS data does not yet exist. We propose a visual analysis pipeline to preprocess the ECG data acquired during concurrent TMS-fMRI and explore the effects of different cognitive tasks and TMS on heart rate.

1.2 Problem Statement

To increase understanding of the effects of TMS modulation and reduce the gap between neuroimaging studies and psychiatric clinical practice, we propose a visual analysis pipeline for research in early stages. In the work of Grosshagauer et al. [2024], the data from concurrent TMS-fMRI have been analyzed, without the additional ECG data. This thesis proposes a framework that supports exploration, comparison, and analysis of TMS and ECG. Cook and Thomas [2005] define visual analytics as "the science of analytics reasoning by interactive visual interface". Combining automated analysis and interactive visualization is also useful in neuroscience, as it supports data exploration of complex healthcare data [Fujiwara et al., 2017; Ganglberger et al., 2019; Jönsson et al., 2020; Li et al., 2012]. Since visual analytics is case-specific in most scenarios [Miksch and Aigner, 2014], a new combination of modalities requires a new visualization and interaction strategy, namely a framework for multimodal TMS and ECG data that supports data exploration and comparisons. The visual analysis design frameworks and models, such as the nested model [Munzner, 2009], Data–Users–Tasks design triangle (D-U-T triangle) [Miksch and Aigner, 2014], and the nested workflow model [Federico et al., 2016], are based on the assumption that the previous workflow in the domain is well-established [Federico et al., 2016] and the tasks are well defined before designing the visual analysis framework [Munzner, 2009]. When research is only emerging, domain experts may not have yet built such previous data processing, workflow as it was in our case with TMS and ECG data. For such early-stage research, integrating the previous workflow approach into the D-U-T triangle [Miksch and Aigner, 2014] would be beneficial to respect the legacy of the data, ease users' adaptability, and ensure tasks compatibility. Building visual analysis pipeline for TMS and ECG data exploration could support the process of understanding the mechanism of action of TMS and empower individualized diagnostic and treatment approaches.

1.3 Aim of the Work

In this thesis, our objective is to provide a multimodal visual analysis pipeline to explore and compare time-oriented high-dimensional data and to support the exploration and derivation of new insights. Our goal is to design and develop a pipeline that enables searching for patterns and comparisons in TMS and ECG-derived data, mainly the heart rate, at different levels of granularity and across time. The visual analytical solution will target to support neuroscientists in their relatively new and correlative workflow by allowing them to explore data, find patterns, and characterize clusters. To do so, existing methodological frameworks in visual analysis D-U-T triangle [Miksch and Aigner, 2014] also need to be adapted to include previous workflow. We aim to answer the following research question:

How can we effectively support the design of a pipeline for the visual analysis of Transcranial Magnetic Stimulation and heart rate data?

1.4 Methodological Approach

Literature Review

Review current studies on multimodal (ECG or TMS) approaches and visual analytics tools for neuroscience. We will also investigate more general approaches for the visual analysis of different types of heterogeneous data, mainly time-varying data to identify appropriate solutions for the analysis and visualization of the involved data types.

Methodological Framework

Prior to task analysis, we extend the D-U-T triangle [Miksch and Aigner, 2014] by also considering the previous workflow approach. The tasks were created based on observation of users in their current workflow of TMS and fMRI data, discussions of users' approach to analyzing the TMS and ECG data, and integration of visual analysis solutions.

T_1 Interactive Data Pre-processing

Pre-processing steps are needed in order to bring the data into a usable format. First, we define the important characteristics of each data modality. Second, we extract the raw data from the machine's output files stored in DICOM format. The ECG leads must be derived from the raw ECG data in order to enable further analysis. Thirdly, each of the data modalities requires appropriate data enrichment. We will verify the completeness and duplicates of the data [Gschwandtner et al., 2012]. We consider different noise-suppression filter designed for ECG data [Makowski et al., 2021; Bota et al., 2024; Pan and Tompkins, 1985; Hamilton, 2002; Elgendi et al., 2010; Emrich et al., 2023]. We validate imputation and noise reduction approaches on synthetic data. We visualize the input and the output of dimensionality reduction and missing-data handling techniques to support decision making and parameter fine-tuning.

T_2 Time-Series Comparison

Time-series data require alignment Ali et al. [2019]. The TMS and ECG data are acquired in different time units and must be converted to the same time domain. As heart rate deceleration is associated with TMS targeting DLPFC Iseger et al. [2021], we need to calculate additional properties derived from the ECG, namely heart rate and heart rate variability (HRV). To see the effects of TMS on the ECG data and heart rate, we perform an automated comparison. We consider statistical tests to correlate the data. To gain insight, we compare the data at different levels of granularity, i.e., different runs (i.e., resting state, decoding, encoding) performed by the participants during acquisition and three different block types, where Transcranial Magnetic Stimulation (TMS) was (non) present under various conditions. We consider other analytical steps depending on the data, such as dynamic time warping Berndt and Clifford [1994] and computing HRV metrics.

T_3 Interactive Visual Analysis

To make interpreting and exploring high-dimensional data easier, dimensionality reduction is beneficial Van Der Maaten et al. [2009]. We applyPrincipal Component Analysis (PCA). When choosing the dimensionality reduction method, we must consider the suitability for the temporal data. Another challenge is to visualize the change in the properties of the data in the same high-dimensional space. We visualize heart rate variability (HRV) metrics in a clustermap.

Design and Implementation

Implementing a new visual analysis solution for neuroscientific data, i.e., TMS, ECG-derived data, according to the aforementioned task analysis as a notebook-based solution for increased usability.

Evaluation

After the design and implementation, we need to assess our work Munzner [2009]. We provide Qualitative Result Inspection (QRI) to assess the value of the developed framework through use-case scenarios Lam et al. [2012].

In the thesis, we elaborate on the evaluation findings along with the methodology used for the analysis of the tasks mentioned above.

1.5 Contributions

In this thesis, we contribute by designing a visual analysis pipeline for early-stage research of TMS and ECG data. The workflow and tasks were not yet established. Therefore, to design the visual analysis pipeline, we have extended the Data–Users–Tasks design triangle [Miksch and Aigner, 2014] by considering and integrating the previous workflow

approach in the analysis. We introduce the Data–Users–Workflow-Tasks design pyramid and assess an additional fourth quality criterion, integrability within designing the pipeline. Within the integrability of the previous research approach, we consider the legacy of data, the adaptability of users, and the compatibility of tasks. Within the visual analysis pipeline, we provide interactive preprocessing steps, including missing data handling and noise reduction, and enable ECG and TMS data explorations, comparisons, and characterization using automated and visual solutions.

CHAPTER 2

Clinical Background

Treatment of mental health problems such as major depressive disorder (MDD) remains a challenge, as about 30% of the patients do not respond to pharmacological treatment [Chen et al., 2023]. This condition is called treatment-resistant depression (TRD) [Chen et al., 2023]. In the United States, the Food and Drug Administration (FDA) has approved Transcranial Magnetic Stimulation (TMS) targeting dorsolateral prefrontal cortex (DLPFC) for TRD and other psychiatric disorders [Tik et al., 2023a]. In real-world studies, 50% to 80% of patients with TRD respond to repetitive TMS treatment [Chen et al., 2023]. The neural mechanism of action of TMS is not yet fully understood [Mizutani-Tiebel et al., 2022]. Section 2.1 briefly introduces the Transcranial Magnetic Stimulation. Two important research domains study the neural mechanism of action of TMS, i.e., Concurrent Transcranial Magnetic Stimulation - Functional Magnetic Resonance Imaging (concurrent TMS-fMRI) (Section 2.2) and Neuro-Cardiac-Guided Transcranial Magnetic Stimulation (Section 2.4). In Section 2.3, we describe how major depressive disorder can be treated by TMS.

2.1 Transcranial Magnetic Stimulation

Transcranial Magnetic Stimulation (TMS) is a non-invasive brain stimulation method. Since 1985, it has not only been used to study brain-behaviour interactions, but it also has promising clinical applications for the treatment of neurological and psychiatric diseases. TMS is based on the principle that the electrical current in a coil induces magnetic fields that enter the skull. In the excitable cortical regions, the magnetic field induces an electric current.[Valero-Cabré et al., 2017] By depolarizing a neuron located near the coil, it can induce action potentials [Mizutani-Tiebel et al., 2022] and generate neurophysiological or behavioral reactions. Depending on the location of the coil, different cortical areas can be affected, e.g. the primary motor cortex. Figure 2.1 shows the TMS coil placed on the scalp. It also visualizes the cortical target [Valero-Cabré et al., 2017].

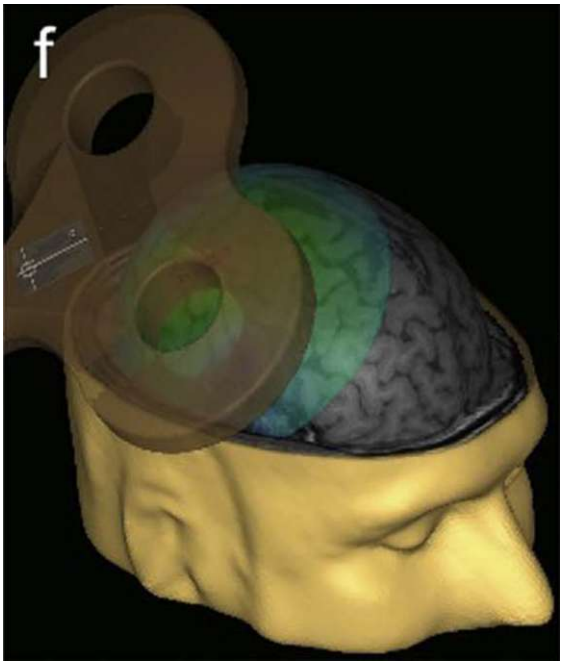

Figure 2.1: Visualization of the TMS coil and cortical target. The figure is taken from Valero-Cabré et al. [2017].

Stimulating the primary motor cortex can induce movement. The minimal energy needed to cause motor movement, specifically the contralateral thumb twitch, is called motor threshold (MT). This amount of electrical energy required for this motor movement has high variability among subjects. To assess the effect of stimulations across various individuals, motor threshold is often employed. The intensity TMS dosings are often expressed as a relative portion to the MT [McConnell et al., 2001].

Via the interconnected pathways of the cerebral circuits, TMS can evoke changes in distant areas of the brain. Among the different TMS modalities, repetitive TMS (rTMS) is a combination of more than two pulses. [Valero-Cabré et al., 2017] Neural navigation and localizing the cerebral circuits are crucial. Currently for localizing dorsolateral prefrontal cortex (DLPFC) the 5cm rule, or the F3 method [Rusjan et al., 2010; Iseger et al., 2017] is used. These methods do not reflect individual variations [Fox et al., 2013]. Finding suitable individualized neuronavigation is important for increasing rTMS efficiency [Iseger et al., 2017].

2.2 Concurrent TMS-fMRI

The simultaneous combination of TMS and fMRI is used to increase the understanding of the mechanism of rTMS-mediated neural modulation. Although other neuroimaging techniques have been used together with TMS, the advantage of fMRI is the exceptional

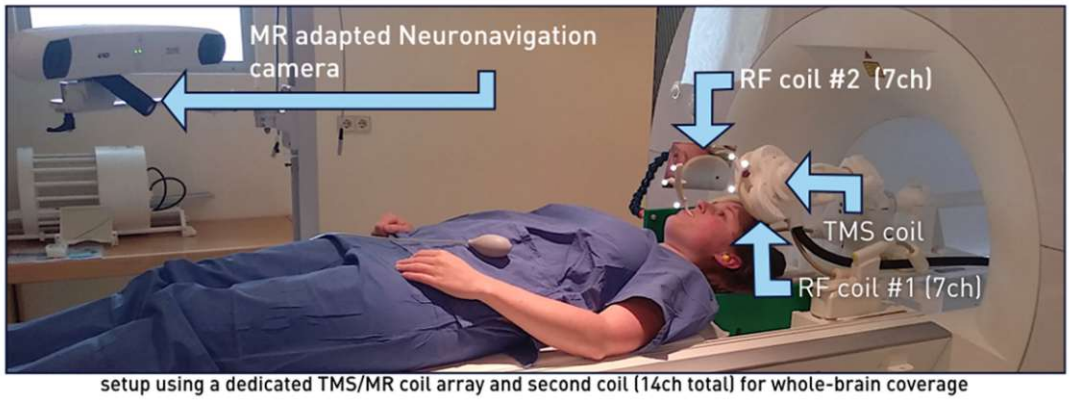

Figure 2.2: Photo of the concurrent TMS-fMRI arrangement by Tik et al. [2023a].

spatial resolution useful to investigate functional connectivity. Since both rTMS and fMRI use a magnetic field, TMS pulses are interleaved with fMRI acquisition to avoid severe artifacts. This process is referred to as concurrent TMS-fMRI [Mizutani-Tiebel et al., 2022]. Figure 2.2 depicts an example of concurrent TMS-fMRI arrangement [Tik et al., 2023a].

Stimulation of cortical areas by TMS can evoke a network effect at connected brain regions. When the pre-motor cortex was stimulated, network effects of the cortico-cortical and cortico-subcortical were visible. Similar induction of remote effects is present during prefrontal TMS. Concurrent Transcranial Magnetic Stimulation - Functional Magnetic Resonance Imaging makes visible the neural correlates of TMS [Mizutani-Tiebel et al., 2022].

One of the challenges of using concurrent TMS-fMRI is the magnetic field interference. fMRI produces images of high quality when the magnetic field is static and homogeneous. TMS coils, as they are heavy metallic objects that induce a magnetic field, affect the field's homogeneity [Mizutani-Tiebel et al., 2022]. To overcome magnetic field inhomogeneities and artefacts, Tik et al. [2023a] introduce the TMS control class that times precisely the TMS pulses and the magnetic resonance scanner trigger signal. There is still a gap between neuroimaging and clinical psychiatric applications. To support the process of diagnosis, prognosis, and treatment of psychiatric disorders, individualized approaches would be beneficial [Ward et al., 2021].

2.3 Major Depressive Disorder Treatment

Despite available treatments such as antidepressants, the first-line treatment, and psychotherapy, depr remains a problem, as 40-50% of patients are resistant to treatment. In the United States, the Food and Drug Administration (FDA) has approved TMS targeting dorsolateral prefrontal cortex (DLPFC) for the pharmacotreatment-resistant major depressive disorder (MDD) and other psychiatric disorders [O'Reardon et al., 2007].

In real-world studies, 50% to 80% patients with the treatment-resistant depression (TRD) respond to the rTMS treatment. Improvement in treatment-responsive patients usually occurs between two and four weeks. [Chen et al., 2023]

One possibility to explain the effects of the rTMS treatment is that rTMS induces neural processes resulting in a similar state of brain connectivity as in fully remitted MDD patients. One network has been identified that appears to exhibit long-term effects following full remission from depression. In this network, there were significant changes in the connectivity patterns between MDD patients undergoing pharmacological treatment and drug-free fully remitted MDD-patients. Comparable brain connectivity alterations were observed in healthy subjects in the same network when comparing brain networks before and after TMS stimulation. Fully remitted MDD-patients and healthy subjects after rTMS stimulation showed similar responses in the same network. This indicates that similar neural networks are present in maintaining a stable and healthy mental state after full remission that can be activated by rTMS [Tik et al., 2019].

Moreover, major depressive disorder is linked with an increased risk of cardiovascular disease, high heart rate, and low heart rate variability (HRV) [Iseger et al., 2020]. Iseger et al. [2020] proposed a frontal-vagal network theory for MDD that connects the brain and heart "that overlaps with functional nodes of the depression network" [Iseger et al., 2020]. The network connecting dorsolateral prefrontal cortex (DLPFC) and subgenual cingulate cortex (sgACC) might explain the clinical response to neuromodulation such as rTMS [Fox et al., 2012; Liston et al., 2014]. Stimulating the vagus nerve (VN) is associated with heart rate (HR) deceleration, as the VN is part of the parasympathetic autonomous nervous system that regulates body functions such as HR and respiration [Buschman et al., 2006].

Furthermore, major depressive disorder is linked with heart rate changes, including increased risk of heart disease [Iseger et al., 2021]. Some studies have shown that TMS decreases heart rate and could stabilize autonomic imbalance [Makovac et al., 2017; Rossi et al., 2016; Udupa et al., 2007].

2.4 Neuro-Cardiac-Guided Transcranial Magnetic Stimulation

A method that combines ECG and rTMS, Neuro-Cardiac-Guided Transcranial Magnetic Stimulation (NCG-TMS), was introduced by Iseger et al. [2017]. The study aimed to confirm the hypothesis that the parasympathetic system is activated after TMS and thus can be used for site-specific TMS. Previous studies had indicated parasympathetic activation as a result of brain stimulation [Makovac et al., 2017; Rossi et al., 2016] showing HR deceleration after stimulation of (sg)ACC and DLPFC [Iseger et al., 2017]. The neuroanatomical framework explaining how the central nervous system is connected to the heart in MDD, was further demonstrated by Iseger et al. [2020]. The first [Iseger

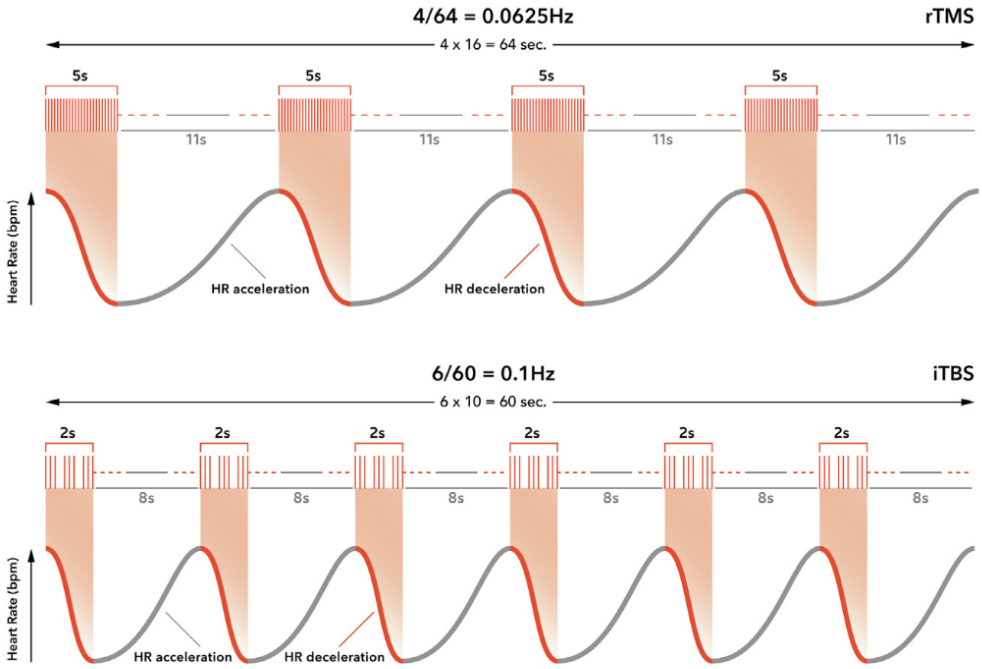

Figure 2.3: Visualization of hypothesized decelerative effects of two different stimulation protocols on HR. Figure taken from Dijkstra et al. [2023].

et al., 2017] and extended [Iseger et al., 2021] results of Iseger et al. indicated that NCG-TMS can be used for individualized neuro-navigation. Furthermore, they show that the motor threshold might not be suitable as the prefrontal excitability threshold. NCG-TMS may be potentially used to determine the adequate stimulation intensity threshold. They studied the immediate response of TMS on the heart rate [Iseger et al., 2017, 2021]. Iseger et al. [2017] used the 10-Hz rTMS protocol Dijkstra et al. [2023]. They have used EEG spots for site-specific stimulation. The heart rate deceleration was spotted for e.g., at F3 and FC3 sites. These sites are commonly used for TMS stimulation [Dijkstra et al., 2023].

Dijkstra et al. [2023] introduce HBC as a measure to identify a suitable TMS target site. The authors called this approach NCG-TMS 2.0. Such target stratification is a promising method for clinical practice. Figure 2.3 shows the repetitive hypothetized deceleration of HR during stimulation [Dijkstra et al., 2023]. Apart from HR, heart rate variability (HRV), the change of HR, changes over time as well. HRV is higher during the resting state than in stressor states [Wachowiak et al., 2015].

2.5 Data

2.5.1 Motivation for Multimodal fMRI-NCG-TMS Data and Currently Available Datasets

Antidepressant outcomes of TMS vary strongly among therapy plans and individuals. Studying the factors, such as individualized TMS intensities, target sites [Tik et al., 2023a; Dijkstra et al., 2023], and state-dependency [Grosshagauer et al., 2024] that influence the antidepressant effects of TMS could increase the success of treatment [Grosshagauer et al., 2024]. Current studies focus on bimodal datasets, i.e., fMRI-TMS [Tik et al., 2017, 2023a; Grosshagauer et al., 2024], and ECG-TMS [Iseger et al., 2017, 2021; Dijkstra et al., 2023].

Combining NCG-TMS with neuroimaging, such as fMRI, could improve our understanding of the mechanism of action of how TMS affects the heart [Jiao et al., 2024] and the brain. Furthermore, using electrocardiogram (ECG) in combination with TMS could help assess the effect of TMS in clinical practice [Dijkstra et al., 2023]. It could help bridge the gap [Ward et al., 2021] between neuroimaging and clinical psychiatric applications. Clinical practice would benefit from individualized approaches in the diagnosis, prognosis, and treatment process of psychiatric disorders [Ward et al., 2021].

For these and other similar applications, providing a systematic pipeline for processing medical and neuroscientific data can support the process of analyzing data and derivation on how these data protocols can be used.

2.5.2 Data Acquisition

Grosshagauer et al. [2024] acquired parallel to chronometric TMS-fMRI ECG data for the same subjects at the same time. 26 subjects were recruited to study how brain state influences the acute effects of TMS in left dorsolateral prefrontal cortex (DLPFC) with connectivity to subgenual cingulate cortex (sgACC) [Grosshagauer et al., 2024].

The experiment was performed in two sessions. The first session was used for neuronavigation and finding the individualized TMS targets [Grosshagauer et al., 2024]. In the second session, data were acquired in different brain-states and three different runs and, i.e., resting state, decoding, and encoding, where ECG was conducted together with concurrent TMS-fMRI. During the decoding and encoding runs, the subjects performed tasks that required memory activation and information recall. To observe state-dependency of TMS effects authors compared fMRI measurements from three different states and two different timings. The chronometric TMS-fMRI experiment is described in detail in Grosshagauer et al. [2024]. The representation of the data acquisition pipeline is shown in Figure 2.4.

ECG data were acquired during the second session simultaneous to the concurrent TMS-fMRI. Of the 26 recruited participants, two subjects were excluded after the first session [Grosshagauer et al., 2024]. The ECG and TMS data are available for the three runs,

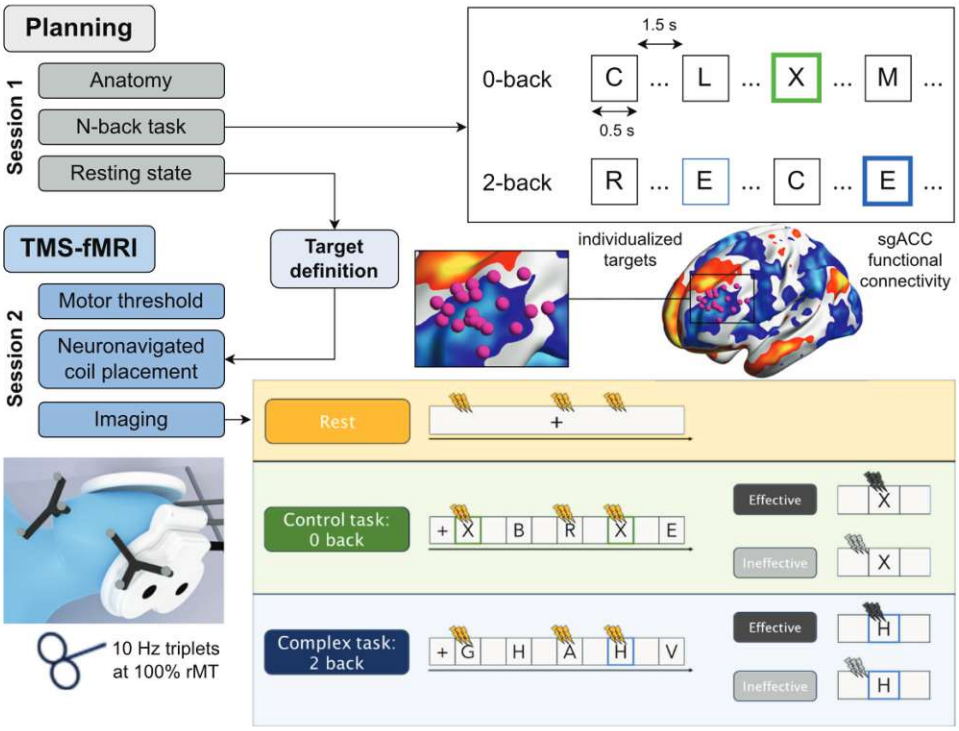

Figure 2.4: Workflow of the concurrent TMS-fMRI experiment by Grosshagauer et al. [2024].

i.e., resting state, decoding, and encoding. The quality of some ECG measurements were evaluated by domain experts as insufficient and were deleted during acquisition. One ECG measurement consists of signals from four electrodes. As currently, the domain experts did not have an existing pipeline for ECG and TMS analysis, in this thesis, we work with ECG and TMS data.

2.5.3 Neuroscientific Hypotheses

According to the review conducted by [Sack et al., 2023], the subject's cognitive, emotional, or perceptual state at the time of stimulation influences the short- and long-term effects of TMS on the brain. In the studies of Iseger et al. [2017, 2021], NCG-TMS was performed to show deceleration of the heart rate at certain stimulation sites as an effect of TMS. A pre-stimulation trough of the RR interval was compared with the first three troughs after the start of the stimulation [Iseger et al., 2021].

Based on the literature, the following hypotheses can be formulated:

H1 The effects of TMS are state-dependent [Sack et al., 2023]. They should differ during the resting state and cognitive tasks.

H2 Heart rate of subject is decelerating after TMS stimulation [Iseger et al., 2017, 2021].

We considered these hypotheses as part of the previous workflow approach when designing the visual analysis pipeline, as we show further in the Chapter 4.

CHAPTER 3

Related Work

In this chapter, we provide an overview of related work. First, we compare the existing NCG-TMS analysis workflow to a medical visualization pipeline Preim and Botha [2013]. Second, we provide an overview of related visual analytics papers.

3.1 Current State of the Visualization Pipeline in Neuro-Cardiac-Guided Transcranial Magnetic Stimulation

As a preliminary study, Iseger et al. [2017] focus predominantly on data acquisition to introduce NCG-TMS. The results were later replicated [Iseger et al., 2021]. The ECG data were acquired at a 1000 Hz sampling rate with co-registration of the TMS impulses that were applied in 10 Hz trains over 5 seconds each at eight different EEG sites. The EEG sites are visualized in the Figure 3.1.

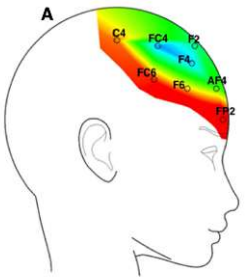

Figure 3.1: Vizualization of Z-scores for different EEG sites using rainbow colormap, with red indicating the HR acceleration and blue indicating the HR deceleratio. The area between the EEG sites has been interpolated. Figure taken from [Iseger et al., 2021].

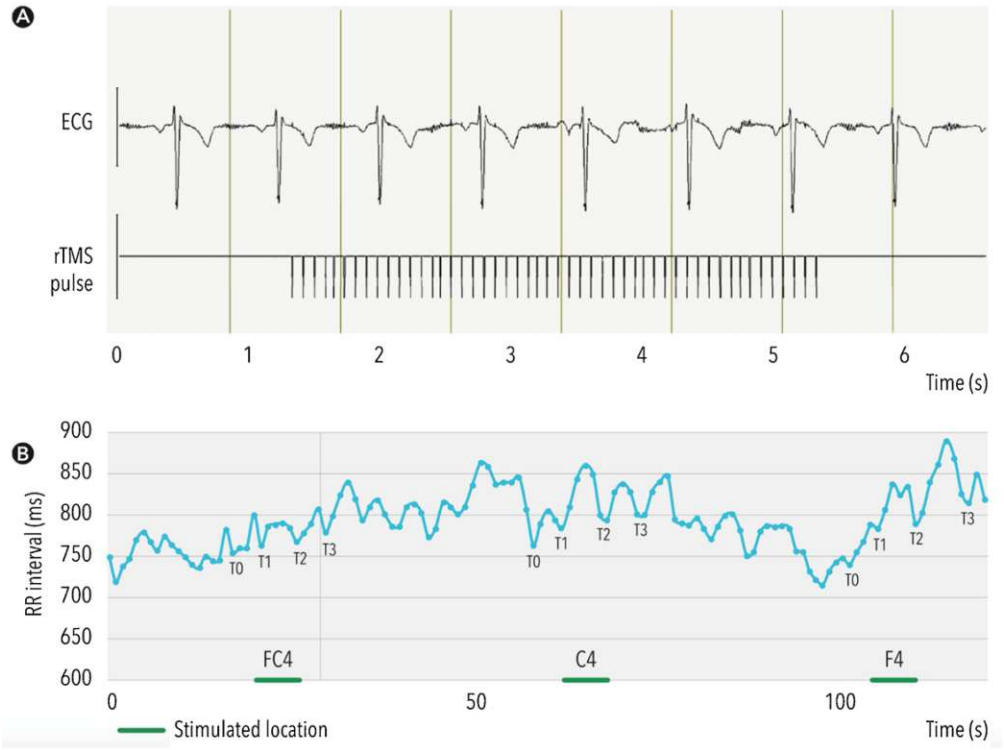

Figure 3.2: Illustration of NCG-TMS analysis. (A) depicts a sample of ECG signal together with TMS impulses in juxtaposition. (B) RR intervals in milliseconds with labeled minimum T_0 prior to stimulation and the three consequent RR minima (T_1, T_2, T_3) after stimulation that correspond to HR maxima and EEG sites as stimulation positions labeled with green underlining. Figure taken from [Iseger et al., 2021].

For data enrichment, R-peaks were detected automatically, and manual inspection and correction was performed for low-quality data. Subsequently, R-R intervals were computed, which builds the basis for heart rate. Figure 3.2A shows a sample of ECG signal during Transcranial Magnetic Stimulation.

To overcome the influence of breathing, the authors used only the HR maxima for data analysis. The HR maximum prior to stimulation (T_0) was correlated to three consequent HR maxima (T_1, T_2, T_3). Sample of the RR intervals with the labeled T_0, T_1, T_2, T_3 are shown in Figure 3.2B. The Z-score was computed as

$$Z\text{-}score = \frac{T_i - T_0}{SD(T_0)}, \tag{3.1}$$

where T_i stands for T_1 - T_3 and $SD(T_0)$ is the standard deviation computed across three stimulations of the same target site applied for normalization purposes [Iseger et al., 2017, 2021]. Z-scores are typically employed in a z-test for substantial datasets of normalized

data when the population mean is established [Gurker, 2018]. This study does not illustrate these scenarios. An improvement could be to test the data for normality.

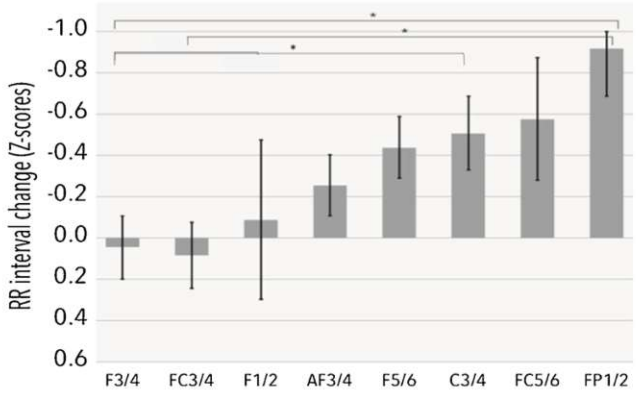

(a) Boxplots of Z-scores for different EEG sites [Iseger et al., 2021].

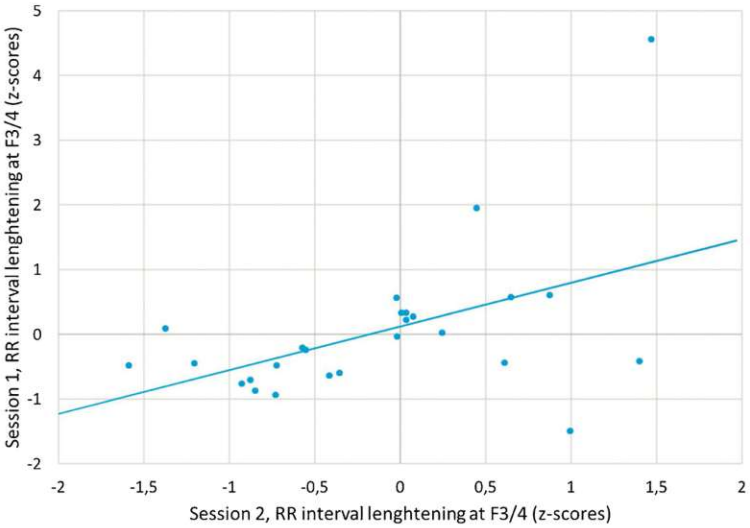

(b) Scatterplot correlating z-scores at EEG site F3/4 in session 1 (y-axis) and session 2 (x-axis) [Iseger et al., 2021].

Figure 3.3: Visualization of Z-score results. (a) Boxplots of Z-scores for different stimulation sites. Inverted y-axis represents increases (upwards) or decreases (downwards) of HR. Positive (bars facing downwards) means the EEG stimulation site was effective. (b) Correlation of z-scores for two sessions in the F3/4 EEG site [Iseger et al., 2021]. Figures taken from [Iseger et al., 2021].

To visualize the results in the paper, the authors used bar plots [Iseger et al., 2017] (Figure 3.3a), scatter plots (Figure 3.3b), and interpolated data for the topographical plot of RR interval change (Figure 3.1) [Iseger et al., 2021]. Figure 3.3a shows group-level

z-scores per EEG site. Positive Z-score values correspond to a larger change in the RR interval which is equivalent to HR deceleration. HR deceleration is a sign of effective Transcranial Magnetic Stimulation.These z-scores were interpolated and depicted with blue color in Figure 3.1 for HR deceleration [Iseger et al., 2021]. As in their case, negative z-scores represent HR acceleration and positive z-scores represent HR deceleration, more suitable than the rainbow color palette would be a perceptually uniform divergent color palette. Scatter plot (Figure 3.3b) correlates two sessions of the same EEG stimulation site F3/4 that was effective for many patients [Iseger et al., 2021].

The data we work with was acquired using a different acquisition protocol. The TMS impulses are not as regular but rather occur in blocks containing TMS impulses during which the subjects perform different cognitive tasks and blocks without TMS impulses. This does not enable the immediate comparison of HR minima before and after the stimulation in our case.

Dijkstra et al. [2023, 2024] used a 10 Hz acquisition protocol and extended NCG-TMS with heart-brain coupling (HBC) to quantify TMS effect on HR. HBC is based on time-frequency analysis Dijkstra et al. [2023]. Figure 3.4 uses a divergent color palette, where red represents increased power that indicates HR deceleration. This approach did not prove to be easily integrable for our work, therefore, it was not considered further.

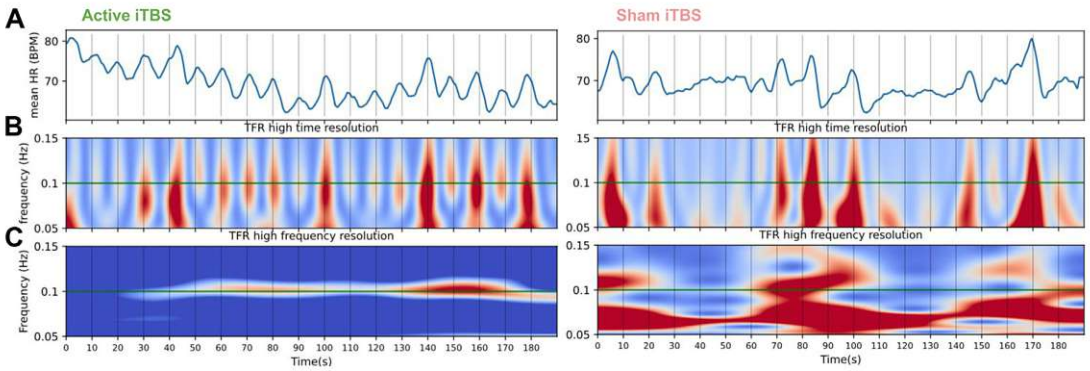

Figure 3.4: HBC report of one session with active (on the left) and sham (on the right) conditions. (A) HR deceleration over time for active stimulation (left). (B) and (C) visualize in red the increased power, which for the active condition corresponds to "repetitive TMS–induced cardiac rhythm of 0.1 Hz" represented with a green line in the middle. Figure taken from Dijkstra et al. [2023].

3.2 Visual Analytics of Medical Data and Time-Varying Data

Although, to our knowledge, visual analytics approaches specifically applied to NCG-TMS data are not available. We present here various steps of visual analytics approaches applied to other fields that could be applicable also to NCG-TMS. The connected domains we looked at were the visualization or analytics of time series data and medical, biomedical, and public health care data.

3.2.1 Pre-processing

Some focus on applying visual analytics in the pre-processing step. Bernard et al. [2012] presented a visual-interactive framework to support building pre-processing pipelines of univariate and multivariate [Bernard et al., 2019] time-series data. This approach enables users to apply their expertise in building the pre-processing pipeline and visualizing the effects of individual routines (Figure 3.5a) Bernard et al. [2012]. Figure 3.5b shows on the left the overview of modules for building pre-processing pipelines, and on the right the visualization module to assess the effects of juxtaposition and dimensionality reduction of input and output, as well as parametrization [Bernard et al., 2019]. We visualized the input and output of the pre-processing steps, mainly the noise reduction methods.

Alemzadeh et al. [2020] focus on missing data in longitudinal cohort data using a visual analysis framework called VIVID. Longitudinal cohort studies collect high-quality information on participants simultaneously over time to monitor indicators such as the incidence and mortality of diseases and medical conditions, including obesity and high blood pressure. Missing data in this manner induces bias, and a proper imputation method is crucial. VIVID supports three tasks, i.e., exploration (Figure 3.6), building an imputation model, and validation of imputations [Alemzadeh et al., 2020]. As in NCG-TMS is emerging, in addition to evaluating different imputation methods, we provide domain experts with the possibility of addressing the missingness problem using complete case analysis.

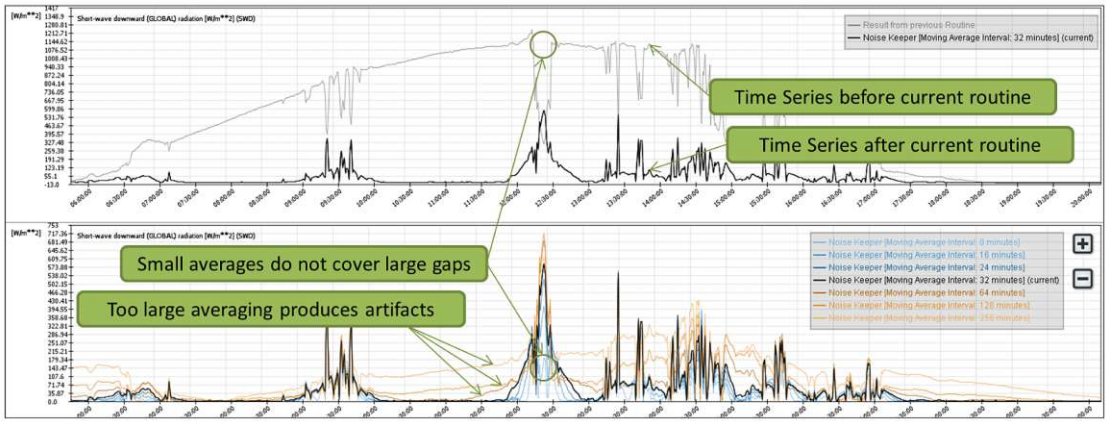

(a) Fine-tuning of noise reduction for univariate time series Bernard et al. [2012]

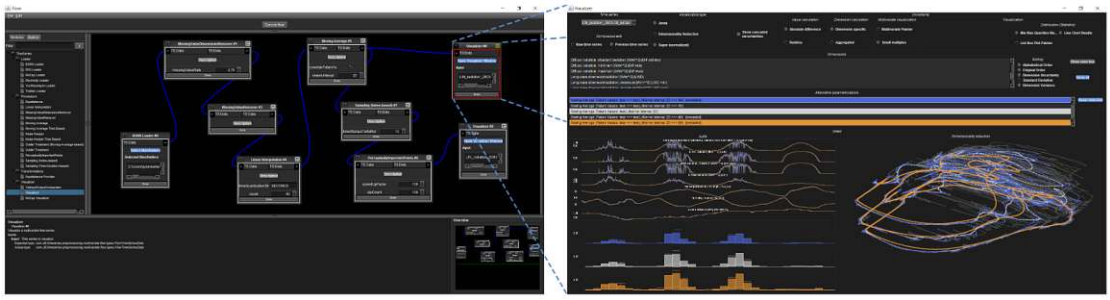

(b) Visual-interactive pre-processing pipeline for multivariate time series data Bernard et al. [2019]

Figure 3.5: (a) Visualizes fine-tuning of moving average interval subtracted from noisy univariate data. In the upper figure, the raw data are visualized together with the effects of one routine, vs. in the lower multiple routines are visualized [Bernard et al., 2012]. (b) The multivariate pre-processing visual-interactive tool. In the window, show how the multivariate pre-processing pipeline can be built and modified. In the right window, the intermediate results were shown using juxtaposition and dimensionality reduction of different parametrizations, color-encoded with blue, light gray, and orange. Figures taken from [Bernard et al., 2012, 2019].

3.2.2 Automated vs Visual Data Analysis

One way to gain knowledge from data is to extract features. In case of ECG data, HRV is often used to get some insight into cardiac autonomic regulation [Billman, 2011]. To measure temporal fluctuations in heart rate, appropriate mathematical estimates should be considered [Frasch, 2022]. Some articles provide an overview of possible metrics and their visualization [Frasch, 2022], while others focus in depth on one Wachowiak et al. [2016]. Frasch [2022] applies the Neurokit2 toolbox [Makowski et al., 2021] with over 100 HRV metrics in three categories i.e. time domain, frequency domain, and nonlinear

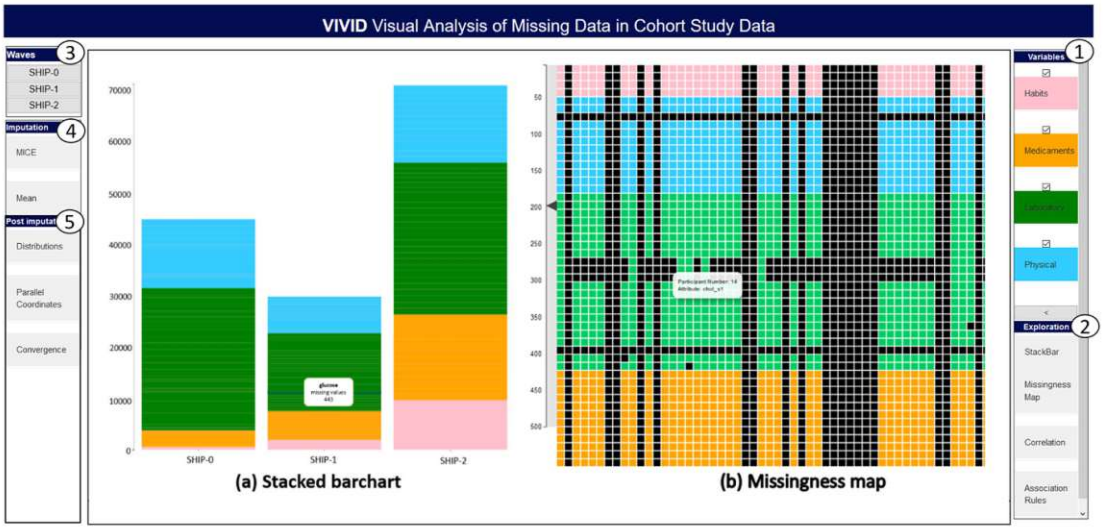

Figure 3.6: Missing data exploration of VIVID interface. It visualizes (a) the number of missing data in different datasets, colour-coded categories of variables, and (b) a missingness map that contains the information of missingness in variables (rows) and participants (columns). [Alemzadeh et al., 2020].

indices, to correlate and visualize the dynamic relationship between HRV and sleep state architecture. Figure 3.7 shows the significant correlations with color-coding [Frasch, 2022]. We also use a range of different HRV metrics. Wachowiak et al. [2016] use user-defined window length and overlap to visualize the continuous wavelet transform that enables time-dependent complexity changes in HRV.

With time-series dimensionality reduction, it is often necessary to investigate correlations. Fujiwara et al. [2021] introduce a visual analytical framework, MulTiDR, with a focus on multivariate time series. MultiDR processes the data in two steps. First, authors project 3D space into 2D space; second, lower dimensions are visualized. In the first step, they use PCA, computing statistical measures, i.e., mean, or unfolding. In the second step, they apply the Uniform Manifold Approximation and Projection (UMAP) [McInnes et al., 2018]. Their results show that PCA&UMAP preserve more variability and show more outliers than Mean&PCA and Unfolding&PCA (Figure 3.8). Under limitations, they mention possible information loss mainly during the first step and possible overwhelmingness of visual scalability by selecting too many clusters [Fujiwara et al., 2021]. In our pipeline, we also used two-step dimensionality reduction. First, we computed different HRV metrics, and then we applied PCA to detect the metrics most contributing to variance in data.

Liu et al. [2022] introduced Multivariate Time Series Visualization (MTV) for anomaly detection in an industrial context. They summarize an ideal human-AI collaboration workflow, characterize design elements of the visualization system, and introduce novel

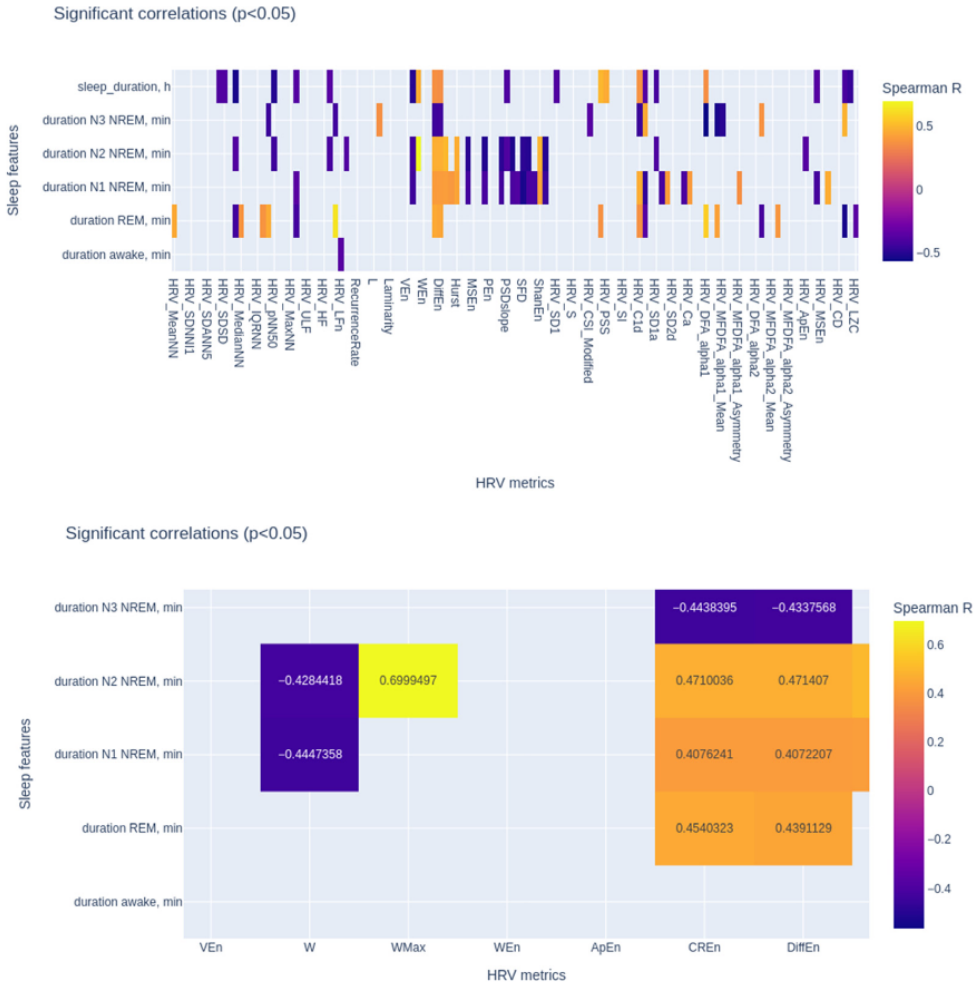

Figure 3.7: HRV metrics correlated with sleep state duration using Spearman R values. Colour-coded are the correlations with $p < 0.05$. In the TOP, all HRV metrics are visualized. In the BOTTOM, a selective zoom is shown for strong correlations [Frasch, 2022].

visualization and interaction techniques. Figure 3.9 shows the MTV interface with signal overview, events, and a side panel, where users can select additional views. In this case, the periodic view was selected [Liu et al., 2022]. This approach is suitable for an industrial context, where the workflow is already well established. In an early-stage research context, as in our case, the workflow of data analysis is only emerging.

Alsallakh et al. [2014] visual analytics approach to support segmenting and labeling time series into intervals. The authors used time-oriented visualizations, such as visualizing raw data with segmented data (Figure 3.10) to allow domain experts to inspect the results and adjust iteratively the parameters and thresholds of automated segmentation [Alsallakh et al., 2014]. We also visualize raw data with adjusted data, especially in the

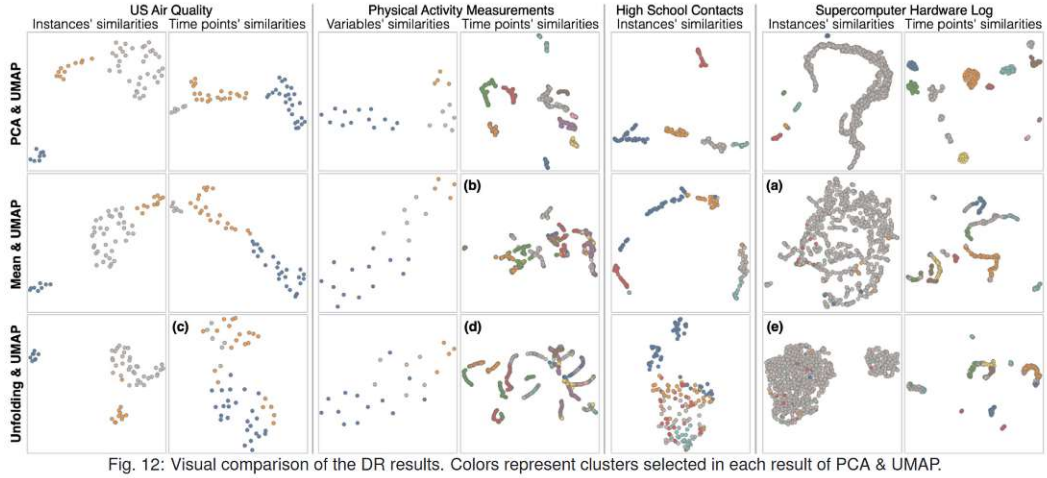

Figure 3.8: Results of the three different two-step dimensionality reduction approaches for different data sets (columns). First row shows PCA and UMAP, second a statistical measure, namely mean and UMAP, and the third row visualizes unfolding with UMAP[Fujiwara et al., 2021].

pre-processing steps.

PerSleep [Garcia Caballero et al., 2021] combines predictive machine learning models for sleep staging and sleep scoring with visual analytics to assess the performance of these models. Figure 3.11 shows the three different views, i.e., patient data, performance, and physiological data with [Garcia Caballero et al., 2021]. Even though, the physiological data are to some extent similar to our data, predictive tasks such as sleep scoring expect the workflow of data analysis in the application domain to be known in advance, and the varying part is the models. In our case, the analysis workflow was only emerging. Therefore, a more comprehensive framework is required to support the establishment of the new analysis pipeline in the neuroscience domain.

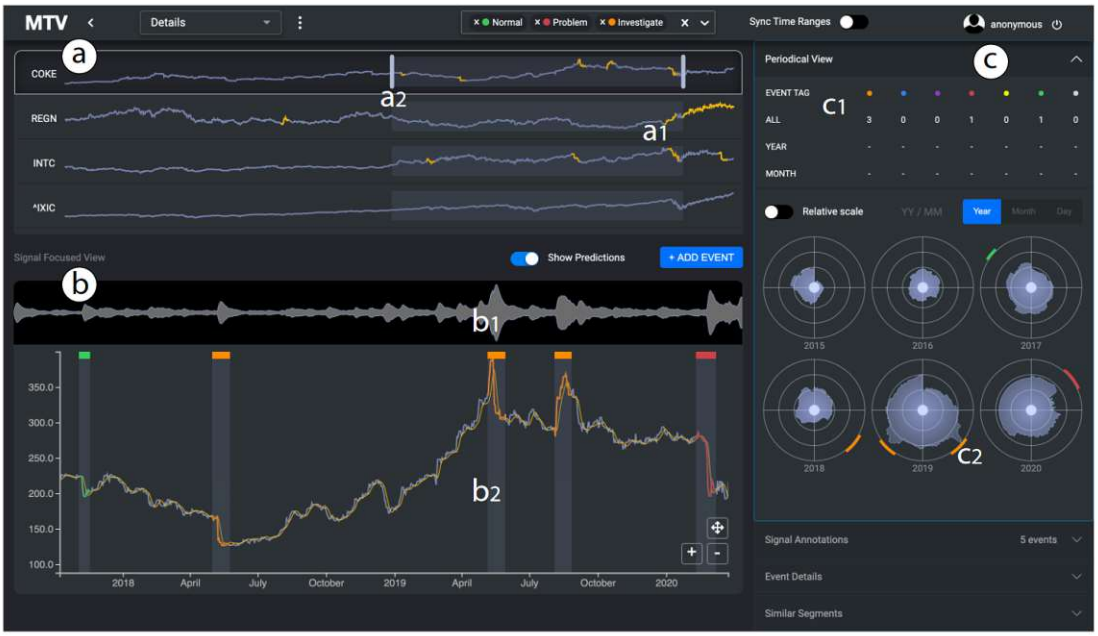

Figure 3.9: MTV interface [Liu et al., 2022] with stock data as an example. Three panel views (a) the Signal Overview, (b) the Signal Focused View with predicted errors in orange to be investigated by humans, (c) Side Panel currently with additional collapsible views, the Periodic View in this case, work synchronized [Liu et al., 2022].

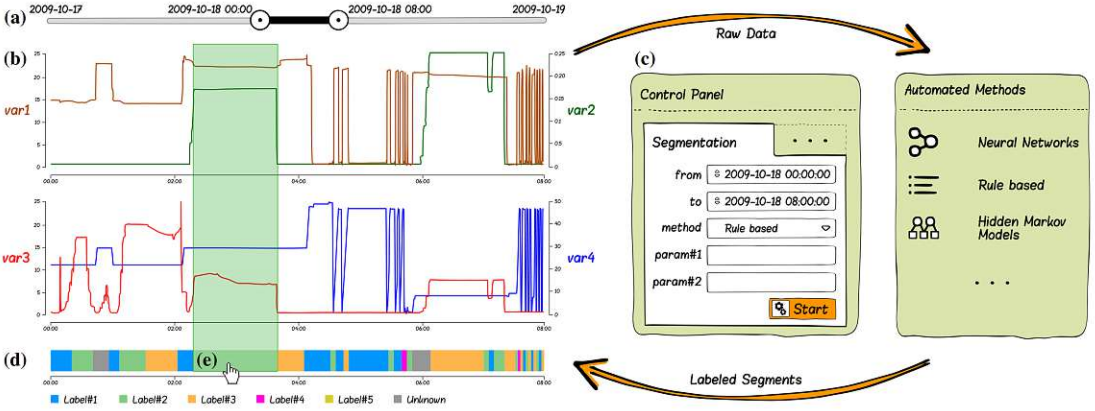

Figure 3.10: Visualization of raw data (b) time-series segmentation (d) automated for chosen time interval (c) Alsallakh et al. [2014].

Figure 3.11: Components of PerSleep: (A) model Selection, (B) patient data views, (C) performance views, (D) physiological data views Garcia Caballero et al. [2021].

CHAPTER 4

Methodology

4.1 Data-User-Workflow-Task Analysis

Miksch and Aigner presented the Data–Users–Tasks design triangle (D-U-T triangle) Miksch and Aigner [2014] to guide the design process of visual analytics. The authors define three main questions to be answered in order to design appropriate visual analytics techniques, i.e.:

(1) "What kinds of data are the users working with? (data)"

(2) "Who are the users of the visual analytics solution(s)? (users)"

(3) "What are the (general) tasks of the users? (tasks)" [Miksch and Aigner, 2014]

However, in research, more data or modalities can often be acquired as they have been analyzed in previous studies. These additional data often require new tasks to be accomplished. In this thesis, we work with ECG and TMS data acquired during concurrent TMS-fMRI acquired by Grosshagauer et al. [2024]. As the primary focus of data acquisition was on previous research, designing a visual analysis pipeline for such early-stage research creates additional challenges. First, users are used to the analysis workflow from previous research that included primarily statistical tests. Second, during the process of designing the pipeline, it was not known what the tasks of the users with the data were. Moreover, the dataset includes elements from prior studies, adhering to specific conventions in which continuity with previous work should be maintained. All of these challenges are connected to the previous research workflow approach.

Additionally, to design a suitable visual representation, it is crucial to understand the current users' workflows Federico et al. [2016] before the integration of visual analytics systems. Scientific workflows Liu et al. [2015] are built of data processing tasks. These

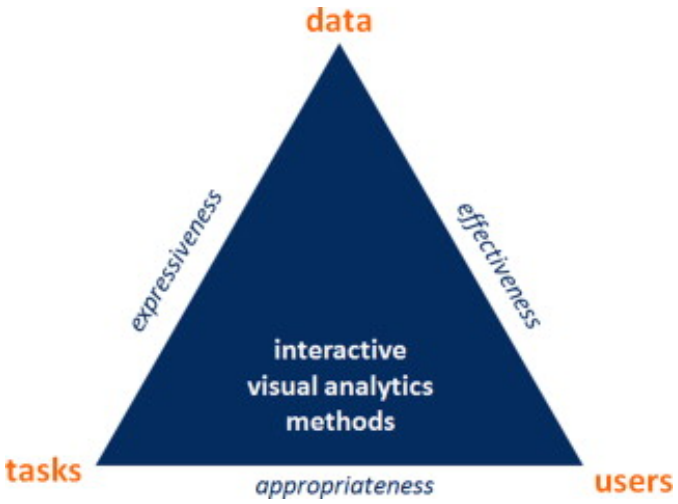

Figure 4.1: The Data–Users–Tasks design triangle introduced by Miksch and Aigner [2014].

tasks are often performed by machines but controlled Federico et al. [2016] and designed by domain experts. A common issue in visual analytics is that users have high expertise in the application domain but might not be used to working with visual analytics Stoiber et al. [2022], which might reduce the success of the newly introduced approaches. For well-established workflows in the application domain, standard approaches to overcome the familiarity gap of users with visual analytics are to provide guidance and visualization onboarding for complex visual analytics solutions Stoiber et al. [2022]. Yet, in our case most important aspect is integrating or taking into account constraints from the previous workflow.

We argue that the previous workflow influences the three main aspects and, therefore, should be considered within the design process of the visual analysis pipeline. In the early stages of research in the application domain, tasks might not yet be clearly defined but rather evolve out of the data investigation process. The data might derive from previous studies, and the previous workflow's approach might strongly influence the users' expectations. For such preliminary research applications, like in our case, we therefore suggest an extension of the three main questions:

(4) What was the previous workflow approach in the application domain? (previous workflow approach)

In this section, we present our proposed Data-User-Workflow-Task Analysis.

4.1.1 D-U-W-T Pyramid

In this subsection, we describe the integration of the previous workflow into the D-U-T triangle (Figure 4.1) [Miksch and Aigner, 2014] from a theoretical perspective. A previous

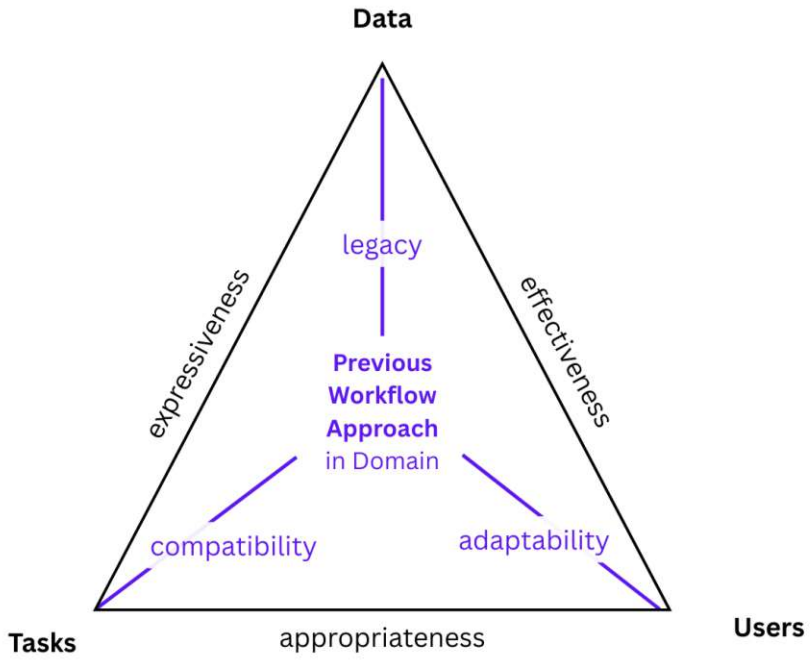

Figure 4.2: Our updated version of the Data–Users–Tasks design triangle [Miksch and Aigner, 2014] for Data-Users-Workflow-Tasks Analysis

extension of the triangle was introduced by Federico et al. [2016]. It incorporates the D-U-T triangle [Miksch and Aigner, 2014] and the nested model [Munzner, 2009]. It is based on the presumption that the workflow in an application domain is already established. This is not applicable for early-stage research, where the workflow is only in the process of evolving. We therefore propose a fourth vertex called the *Previous Workflow Approach*, considering that the integration of the previous research workflow might be especially useful in two situations. First, when a new data modality is to be involved, and therefore the previous workflow is not sufficient per se, as it was in our case. The other is when the existing workflow is to be improved, and (new) visual analysis components are to be integrated. To include both of these scenarios, we refer to the fourth vertex of the pyramid (Figure 4.2) as the previous workflow approach.

The D-U-T triangle names three major quality criteria shown as edges in Figure 4.1 that the visualization must satisfy. **Expressiveness** refers to the edge between Tasks and Data and requires the visualization to be truthful to the data, i.e. to visualize precisely the data's content. **Effectiveness** focuses on the interaction of users with the data. It requires that the visualization takes advantage of the human visual perception system and the user's cognitive capabilities. To fulfill **appropriateness**, the cost-value ratio needs to be considered Miksch and Aigner [2014]. We introduce a fourth criterion, i.e., **integrability**, according to which, a meaningful visual analysis solution for early-stage research applications should consider and integrate the previous workflow approach. A

visual analysis framework should preserve important parts of the previous research, but extend the previous workflow with visual analysis solutions. The integrability criterion with respect to data, users, and tasks consists of three subcriteria, i.e., *legacy* (between Data and Workflow), *adaptability* (between Users and Workflow), and *compatibility* (between Tasks and Workflow) (Figure 4.2).

Legacy of Data When designing a visual analysis framework, the continuity of the data should be preserved. Data comes in a given format, which might affect the lower levels of visualization creation as defined by Munzner [2009], mainly encoding techniques and algorithm design. There might even be a direct connection to the previous workflow. Data might directly come from previous research, but something new is aimed to be investigated, or more data might have been collected than previously analyzed. *Legacy* of the data (Figure 4.2) should be considered.

Users' Adaptability Visual analysis frameworks are built for users; however, users bring practices from their domain of expertise. These practices might not be compatible with the new framework, or the expectations on the visual analysis framework are, to a large extent, based on their previous workflow approach. The workflow's *adaptability* to the user's needs (Figure 4.2) should be considered while designing the visual analysis framework.

Tasks' Compatibility The design of the new visual analysis approach should offer possibilities for a new or better task execution. Within the design of the visual analysis framework, the components of the previous workflow should be considered and, if appropriate, integrated into the new workflow. A new visual analysis framework should be *compatible* (Figure 4.2) with the tasks of the previous workflow in the application domain.

4.1.2 Data Characteristics

In this thesis, we combine the benefits of generated data with measured data. The measured data were collected as part of a previous study Grosshagauer et al. [2024], aimed at moving towards a trimodal analysis of the effects and mechanisms of TMS. We used generated data to evaluate the accuracy of pre-processing steps. Generated data can be used as ground truth to distinguish the effects of processing steps. The results of analyzing genereted data were afterwards applied to a real-world application to study the effects of TMS on heart rate (HR) in three different runs.

Generated Data

We use synthetic 1-channel ECG data with generated noise to measure and evaluate the individual steps of the processing pipeline. According to data typology, these generated ECGs are continuous numerical data with 2D attributes, i.e., time and intensity, in a 1D space. To generate the data, we applied two approaches. We generated the data with

two different approaches, i.e., the Daubechies wavelets Daubechies [1992] and ECGSYN McSharry and Clifford [2003] (Figure 4.5). ECGSYN, unlike previous approaches, focuses on simulating realistic human physiology, such as the breath cycle, influencing ECG McSharry and Clifford [2003].

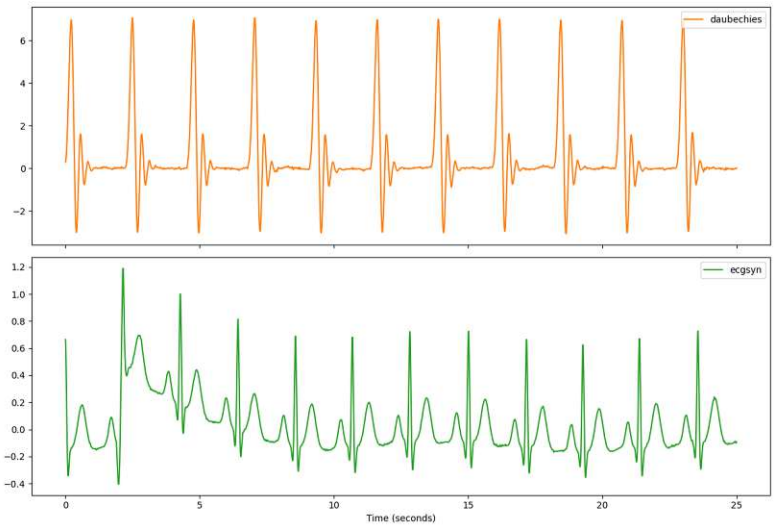

Figure 4.3: The Daubechies wavelets Daubechies [1992] and ECGSYN McSharry and Clifford [2003] for synthetizing ECG data.

Measured Data

The measured data was acquired by Grosshagauer et al. [2024]. In this thesis, we work with TMS and ECG data. Of the 26 recruited subjects, we only consider those where both TMS and ECG are available for the run, i.e. decoding, encoding, and resting state. Figure 4.4 shows TMS signal interleaving the noisy ECG data.

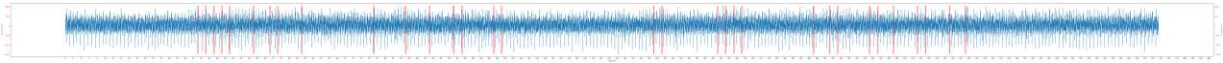

Figure 4.4: Raw data of subject P04 for resting state run. Noisy ECG data are color-coded with blue. Red vertical lines represent TMS impulses. These impulses were acquired in triplets but logged were only the starting and the end point of the triplet.

TMS measurement was divided into periods of 3 different blocks. The third block represents time periods without TMS. In other blocks TMS impulses were coupled into triplets with very short time difference. The data are nominal with a 1D attribute in a 1D space. Every subject has constant impulse intensity throughout for each run that corresponds to the resting motor threshold. The aquisition setting is shown in Figure 2.2.

ECG raw data were acquired with 4 electrodes. According to the recommendation of the domain expert, we used only one ECG lead gained from the subtraction of channel 1 from channel 4. Therefore, the data consist of 2D attributes, i.e., time and intensity, in a 1D space.

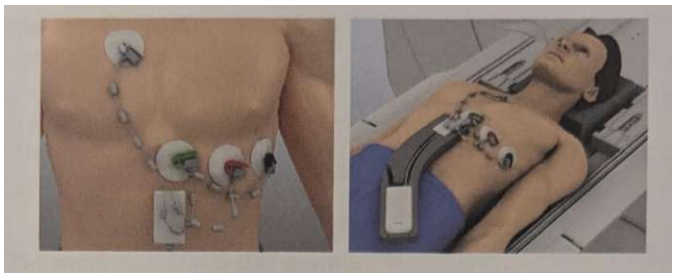

Figure 4.5: ECG electrode positions based on the Syngo MR E11 operating manual. Figure provided by Martin Tik.

4.1.3 Users

Our visual analysis pipeline targets domain research that works with high-dimensional, time-oriented medical data such as ECG. In a narrower sense, we focus on brain stimulation researchers as we apply our processing pipeline on measured TMS-ECG data. They are interested mainly in investigating heart rate changes across different patients and runs. In a broad sense, our processing pipeline is beneficial for other domain experts interested in the systematic processing of time-oriented data such as ECG.

4.1.4 Previous Brain Stimulation Research Workflow

Previous Workflow

Currently, they have a well-established concurrent TMS-fMRI analysis pipeline. With this pipeline, the domain experts had already published several papers to study the intensity of stimulation (Figure 4.6) [Tik et al., 2023b,a] and the stimulation sites (Figure 2.4) Grosshagauer et al. [2024]. Their approach consists of two sessions, i.e., planning and concurrent TMS-fMRI with cognitive tasks execution. In the first session, the anatomy of the head and brain is scanned MRI Tik et al. [2023a]; Grosshagauer et al. [2024]. We observed the second session of one subject, where TMS impulses were interleaved with fMRI. Within their data processing, they used Matlab-based SPM12 and Python. A general linear model was used to quantify the voxel-wise BOLD response. To test for statistical significance, the percent signal change (PSC) was calculated for the regions of interest. One-sample t-tests and paired t-tests were applied to the mean PSCs [Grosshagauer et al., 2024].

We observed their current workflow and discussed their ideas for future workflow. At point of design the visual analysis pipeline domain experts were missing a workflow to process ECG data and to compare HR and TMS data. In this thesis, we therefore focus

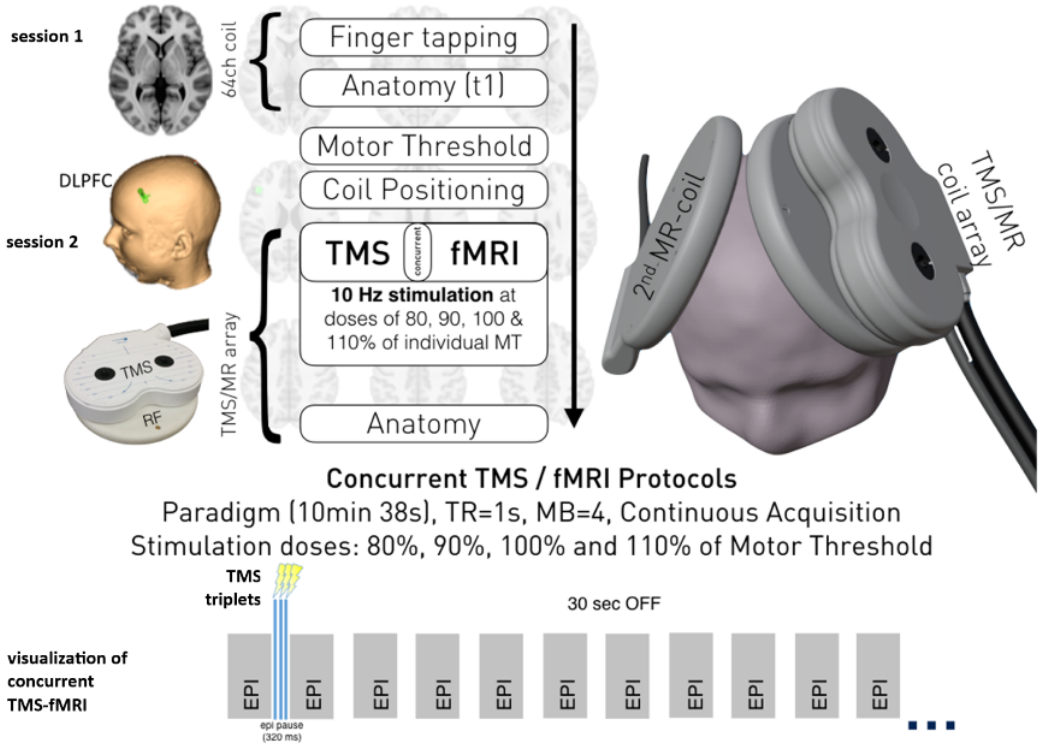

Figure 4.6: (TOP) Workflow of the concurrent TMS-fMRI experiment of different stimulation intensities and image of coil-positioning. (BOTTOM) Visualization of triples of TMS interleaving the EPI slices in fMRI acquisition. Figure adapted from Tik et al. [2023a].

on building a visual analysis pipeline that would be integrable in the future with their previous concurrent TMS-fMRI workflow.

Approach Based on Previous Workflow

In this subsubsection, we describe, based on discussions with domain experts, how they would approach to analysis of a new data modality, i.e. ECG mainly HR and comparisons of HR with TMS. We considered their approach based on their previous research workflow within the process of defining tasks and designing the visual analysis pipeline, mainly by designing a visualization of results.

Based on the experiment, two main levels of granularity are of interest for domain experts, i.e., runs and blocks. Figure 4.7 shows the three different types of runs, i.e., decoding and encoding, during which cognitive tasks (Figure 4.7a) were performed. In the paper of Grosshagauer et al. [2024], the authors refer to different runs as cognitive states or sometimes cognitive tasks. To avoid confusion with tasks from D-U-T triangle, we had

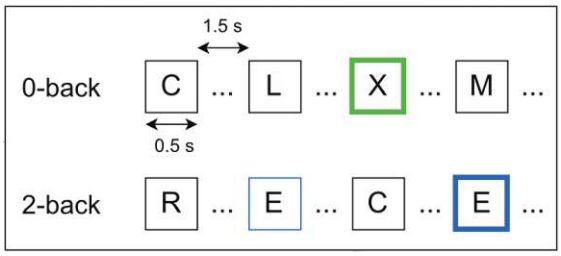

(a) Two different cognitive tasks. 0-back acts as an active control cognitive task, where the subject has to press a button whenever a certain letter is visible. The 2-back cognitive task involves activating memory, as if a certain letter appears more than once, a button should be pressed.

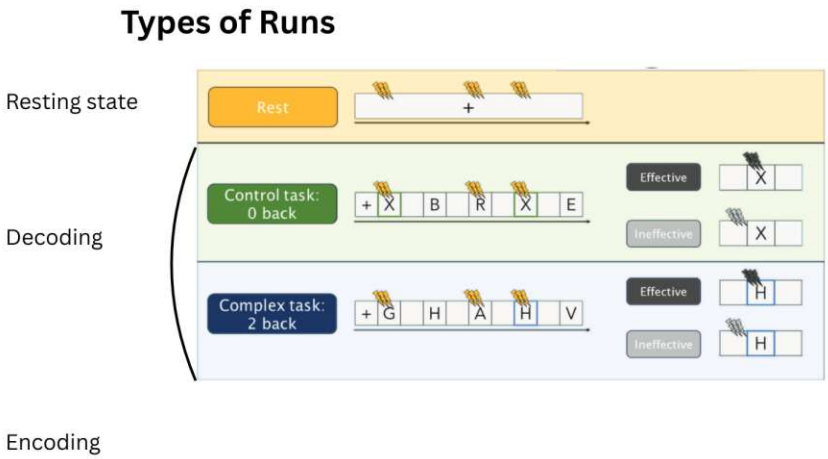

(b) Three different types of runs are resting state, decoding, and encoding.

Figure 4.7: In the paper of Grosshagauer et al. [2024], two different cognitive states were i.e. resting state and decoding. During the decoding run, the cognitive tasks described in (a) were performed. ECG was measured during the whole scope of measurement of one run. Additionally, the encoding run was measured during the same experiment but these data were not included in the paper. Figures were adapted from Grosshagauer et al. [2024].

agreed with domain experts on the term run for these three different cognitive states. Each of the runs was further divided into blocks based on the TMS settings.

Step 1: Data Overview As the research of NCG-TMS, especially during the concurrent TMS-fMRI protocol, is emerging, it is helpful to acquire a general understanding as an initial step. The data overview might detect possible measurement errors, where the heart rate values are in an unexpected range. Brain stimulation researchers, therefore, start the data investigation by computing simple statistical measures such as mean and standard deviation. Additionally, observing the data distribution might indicate some

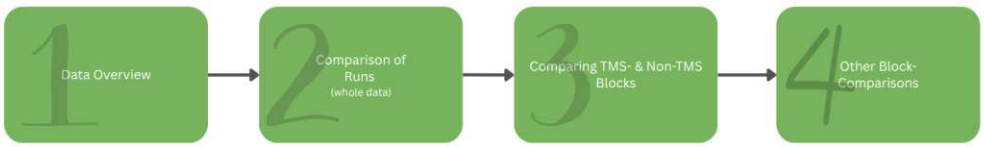

Figure 4.8: Neuroscientific Research Pipeline

insight into inter- and intra-subject variance.

Step 2: Comparison of Runs Domain experts prefer to start their analysis by comparing the whole HR data for one subject and run without further division. This enables comparison of different runs.

Step 3: Comparing TMS- & Non-TMS Blocks After analyzing the data as a whole, more detailed exploration follows. As the TMS impulses were grouped into blocks with and without TMS impulses, domain experts chose to use the different TMS blocks as means to evaluate the effect of TMS on HR. As blocks 1 and 2 contain TMS impulses, a lower HR is expected for these time periods than for block 3, where supposedly no TMS impulses are present. This expectation is based on previous research Iseger et al. [2017, 2021]; Dijkstra et al. [2023] that indicates heart rate deceleration after TMS impulses.

Step 4: Other Block-Comparisons Other comparisons are not the primary focus of the domain experts. Despite that, exploring other possible relations in the data, e.g., comparing block 1 with block 2, is of interest.

4.1.5 Tasks

Munzner [2009] defined the nested model for visualization design and validation to characterize tasks. The model is based on the assumption that before designing the visual analytics framework, tasks should be well defined Munzner [2009]. This might not be the case in the early stages of domain research, especially for the lower-level domain and abstract. For individual tasks, it might not yet be clear what, why, and how Brehmer and Munzner [2013] the data should be analyzed. To support early stages of research, we combine approaches that domain experts used from previous studies' workflows, such as statistical tests, with further visual analytical approaches, clustering, to support data exploration.

T1 Interactive Pre-processing

For further visual analysis of the raw electrode data. ECG data are computed as electrode difference and therefore ECG lead must be calculated from the electors. We need to make sure there are no inconsistencies in the data.

T2 Time-Series Comparison

TMS and ECG were acquired simultaneously. We want to explore the effects of TMS on the HR. We want to see structures in the data, characterize subgroups of the signals and find possible patterns.

T3 Interactive Visual Analysis

We want to enable users to gain insight from the data. We want to enable visual exploration and analysis of patterns in the signal.

4.1.6 Quality Criteria

Expressiveness Expressiveness requires that the visual encoding makes the influence of preprocessing steps on the data transparent. Our visual analysis pipeline should highlight differences and characterize subgroups in the data. The design of the pipeline should also facilitate the visual exploration and detection of possible patterns in the data.

Appropriateness Appropriateness concerns the fit between analytical tasks and the evolving needs of domain experts. In brain stimulation research, experts often refine their questions during exploration. To account for this dynamic process, the visual analysis pipeline should be highly flexible and adaptive. An exploratory approach would enable users to employ their visual cognitive skills in gaining an overview of the data and investigating patterns.

Effectiveness Effectiveness emphasizes enabling meaningful interaction with the data. The visual analysis pipeline should provide tools that allow users to analyze the TMS and ECG data. Users should be able to interact with the data by exploring different subgroups and gain insight into the characteristics of these subgroups.

Integrability The fourth criterion, i.e., integrability in our case, requires that the visual analysis pipeline is implementable into the future trimodal fMRI-ECG-TMS data analysis pipeline. More concretely, the *legacy* of the data, users' *adaptability*, and tasks *compatibility* need to be considered. Data are derived from previous research with a focus on fMRI-TMS analysis and come in domain-specific formats. ECG data come in DICOM format in binary encoding, stored in a device-specific custom tag. Users' expectations are strongly linked to their previous research, especially to statistical tests, as such the users' *adaptability* must be taken into account. Finally, tasks were defined by users only

at a high level based on previous research. The tasks of previous research and high-level hypotheses in the domain should be considered to what extent they are *compatible* with the current data and new modality combination, i.e., ECG and TMS.

4.2 T1 Pre-processing

In this section, we describe the pre-processing steps. To build a pre-processing pipeline, we test and validate different imputation and noise reduction approaches on generated data. For measured data, we start with data extraction, followed by handling the missing data by providing an option to choose between complete case analysis and an imputation method.

4.2.1 Data Extraction

Much of the medical data is stored in Digital Imaging and Communication in Medicine (DICOM) files. DICOM is a standardized format for imaging data such as CT, MRI, SPECT, PET Mustra et al. [2008], but has also been used for ECG data Bond et al. [2011]. In 2000, the DICOM Supplement 30, waveform extension, was proposed for biomedical signals, including ECG, which uses binary encoding Bond et al. [2011]; Trigo et al. [2012].

Generating Synthetic Data

The Daubechies wavelets [Daubechies, 1992] are a common transform to simulate ECG data due to their similarity to ECG features Saritha et al. [2008]; Balachandran et al. [2014]. Later, ECGSYN [McSharry et al., 2003; McSharry and Clifford, 2003], a dynamic model consisting of three ordinary differential equations, was introduced to simulate ECG signals in a 3D space. To generate realistic human ECG, physiological phenomena such as respiratory sinus arrhythmia were simulated [McSharry et al., 2003]. Breath cycles affect the HR. Respiratory sinus arrhythmia describes the interaction of the cardiovascular and respiratory systems [Pham et al., 2021]. The samples of the two ECG generating approaches are shown in Figure 4.5. As the purpose of our pipeline is processing measured human data containing fluctuation, we predominantly use the ECGSYN model for generating data. However, we allow users to choose between the Neurokit [Makowski et al., 2021] implementations of Daubechies wavelets and the ECGSYN dynamic model. To make the synthetic and measured data compatible, we used the same sampling frequency of 400 Hz as in the measured data.

Measured Data

The measured data we were given were stored in DICOM format under a custom tag (7FE1, 1010). Under this tag, different physiological log files were encoded in bytes using ASCII encoding, together with the names of the log files. As the log files have a form of a table, we stored the decoded data in a CSV file. One of the files contains ECG data.

Due to the uncertainty regarding whether recordings of additional physiological data, such as respiration and pulse, were indeed captured from the subjects, this thesis focuses solely on working with ECG data. ECG data consist of acquisition time tics and four electrode measurements. According to the recommendation of the domain expert, we used only one ECG lead gained from the subtraction of channel 1 from channel 4. The domain expert conveyed that the ECG data was recorded at a sampling rate of 400 Hz.

Implementation

ECG data was stored in the DICOM files in binary encoding. After decoding, we observed the log file had a tabular form, where the columns were acquisition ticks that represented the time of the value acquisition, name of the electrode (ECG1 - ECG4), and the intensity value. We converted the log to enable missing data identification. We stored the dataframe as csv file. The ECG data were acquired using four electrodes; therefore, the raw data were stored in four channels. In the application domain a popular format is EDF. We implemented, therefore, an export of the data into this format.

4.2.2 Data Missingness

According to RUBIN [1976] classification of the missing data problem, there are 3 categories, i.e., missing completely at random (MCAR), missing at random (MAR), and missing not at random (MNAR). In the MCAR category, every data point has the same probability of being missing, whereas MAR deals with data missingness with the same probabilities within groups of observed data. MAR is the most common assumption to start with. An example can be a weighing scale. If the weighing scales are placed on different surfaces and there is no significant difference in the number of missing values, it would be considered as MCAR. Placing weighing scales on a soft surface can results in more missing data. In this case, it would be MAR as the surface type is known, and we might suppose that the missingness within the surface type is MCAR. For data not missing at random, the causes of data missingness are related to the data, but the cause might be unknown. Public opinion research with less frequent responses for weaker opinions exemplifies MNAR van Buuren [2018]. Little Little [1988] introduced a test to distinguish MCAR from MNAR and MAR.

There are two main approaches to handling missing data: complete case analysis (CCA) (or listwise deletion van Buuren [2018]) and imputation. The samples with missing data are ignored using CCA, while being replaced using imputation Alemzadeh et al. [2020]. The missing data problem occurs in many studies with a wide variety of topics [Hand et al., 1993]. The method of handling missing data is not always mentioned in studies. The most common approach is data deletion, which sometimes occurs silently van Buuren [2018].

Imputations for Generated Data

We simulated missing data by deleting some data points from the ECG. In generated data, the missingness occurs completely at random. We used seven different deletion rates, i.e., 0.001, 0.002, 0.005, 0.01, 0.05, 0.1, 0.2. We used the same frequency of 400 Hz. We test different imputation methods. In many applications, it is critical to consider computational efficiency apart from estimated accuracy to find an appropriate imputation method. Usually, with increasing algorithmic complexity, the computational cost also increases, even though accuracy is typically higher Ding et al. [2020]. We therefore included some basic imputation methods, such as mean, median, Last Observation Carried Forward (LOCF), and Next Observation Carried Backwards (NOCF), considered by van Buuren van Buuren [2018] as ad hoc solutions. Linear interpolation can be used as an imputation method with good results for time series Steffen et al. [2015]. Steffen et al. Steffen et al. [2015] tested different R implementations of imputation methods. Linear interpolation was the most accurate of the imputation methods tested, and LOAF was the most computationally efficient Steffen et al. [2015]. Apart from linear interpolation, we also tested polynomial interpolation. To ensure no remaining NaN values even at the beginning and end of the time-series, both for linear and polynomial interpolations, we applied additionally LOCF and NOCF imputations for possible remaining NaN values.

Measured Data

We apply Little's MCAR test Little [1988] on the data to categorize the missingness type. Categorazing the missingness supports the decision making of appropriate imputation method [van Buuren, 2018]. We enable users to choose between the complete case analysis and an imputation method.

4.2.3 Noise Reduction

The acquisition of ECG is often associated with various types of noise. This noise can arise from a variety of sources, including baseline wander, powerline interference, and electrode motion artifacts [Kher, 2019]. The acquisition of ECG is connected with noise. We provide a visual inspection of the design techniques. We evaluated two common noise sources, i.e., baseline wander and powerline interference [Singh et al., 2019]. This evaluation is conducted by simulating these noises and adding them to simulated ECG signals similarly to those shown in Figure 4.9.

Different approaches to suppress noise in the ECG data include conventional filtering techniques, empirical mode decomposition (EMD), deep learning encoders, wavelet-based models, Bayesian filter models, and visibility graph models. Conventional filtering includes high-pass and low-pass filters [Makowski et al., 2021], a finite impulse response (FIR) filter [Bota et al., 2024], and some conventional approaches focus on QRS detectors and ECG feature extraction [Pan and Tompkins, 1985; Hamilton, 2002; Elgendi et al., 2010]. EMD-based models involve decomposition into intrinsic components. These models are sensitive to selecting an appropriate intrinsic mode signal, yet they perform

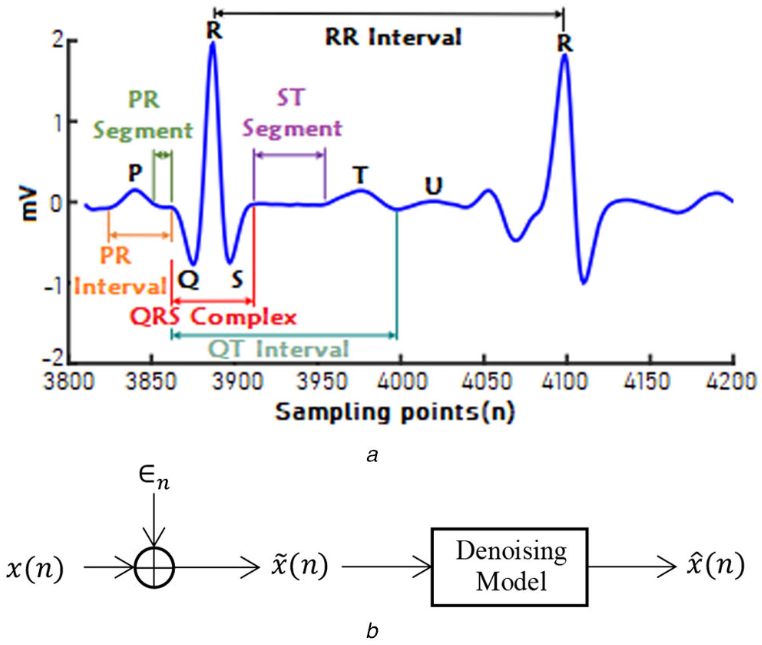

Figure 4.9: Figure "Denoising mechanism of a typical cardiac cycle" taken from Chatterjee et al. [2020]. (a) Typical cardiac cycle of ECG signal with labels. (b) Visualization of noise reduction mechanism, where to clean ECG $x(n)$, $\in_n$ is added to create a noisy ECG $\tilde{x}(n)$.

well for baseline wander and muscle artifacts. Deep learning approaches are suitable for applications where a large amount of training data and ground truth is available. As we have a limited amount of data, this approach was, in our case, not applicable. Wavelet-based models are based on a discrete wavelet transform. They require careful selection of mother wavelets for ECG signal decomposition. These models are effective for Gaussian noise. Bayesian filter models are based on Bayesian estimation that incorporates prior knowledge into new measurements [Chatterjee et al., 2020]. The visibility graph-based model introduced by Emrich et al. [2023] focuses on R-peak detection. Minimum distance peak distance is set to 300 ms. If there is more than one candidate with a closer proximity, as R-peak is chosen, the one with the highest weighted signal Emrich et al. [2023]. If the noise signal interferes with the R-peaks, this approach might not be suitable.

An implementation was not available for every denoising technique. In this thesis, we there applied and tested the Neurokit2 [Makowski et al., 2021] implementation of noise removal techniques.

- Neurokit2 [Makowski et al., 2021] implementation of 0.5 Hz high-pass butterworth filter of fifth order combined with powerline filter,
- Neurokit2 adaptation of Biosspy FIR filter [Bota et al., 2024] of $1.5 * samplingRate$

order with lower cutoff frequency of 0.67 Hz and higher cutoff frequency of 45 Hz. With the assumption of a minimal heart rate of 40 bpm.

- QRS detector [Pan and Tompkins, 1985] using high-pass and low-pass filters
- ECG analyzer with high- and low- frequency noise description [Hamilton, 2002]
- QRS detector using a second-order Butterworth filter [Elgendi et al., 2010]
- R-detector based on visibility graphs [Emrich et al., 2023].

4.3 T2 Comparisons

Time-series data require alignment Ali et al. [2019]. The TMS and ECG data are acquired in different time units and must be converted to the same time domain. Based on the previous workflow approach of domain exports, we apply statistical tests to the data. To see the effects of TMS on the HR, we measure similarity using Dynamic Time Warping (DTW) and compute over 80 heart rate variability (HRV) indices across the three block types (including TMS - and non-TMS - blocks) and three runs, i.e., resting state and cognitive tasks. Domain experts were used to working with statistical tests; we included statistical tests. Similar to Fujiwara et al. [2021], we provide a two-step dimensionality reduction. First, we compute different HRV metrics, then we apply PCA.

4.3.1 Statistical Test

As domain experts are used to correlating the data with statistical tests, we started comparing the data in this manner. First, we tested the data for normality using the D'Agostino-Pearson test D'Agostino and Pearson [1973]. Based on the normality result, we apply statistical tests. We implemented the statistical tests for both cases. If the data are normal, we apply a t-test to correlate two time series or an ANOVA for multiple time series correlation. For non-normal data, we applied the Mann-Whitney test for two time series and the Kruskal-Wallis test for correlation of multiple time series Belciug [2022]; Okoye and Hosseini [2024].

4.3.2 Dynamic Time Warping

Dynamic Time Warping (DTW) is a technique introduced by Berndt and Clifford [1994] that quantifies the degree of alignment of two time series. In temporal data, patterns can occur at different rates. DTW can find patterns even if the time axis is stretched or compressed. Therefore, this approach is suitable for measuring similarity in real-world temporal data Berndt and Clifford [1994] such as heart rate. As this approach is computationally heavy, later papers attempted to optimaze DTW to reduce the complexity [Salvador and Chan, 2007] and enable multi-dimensional comparisons [Shokoohi-Yekta et al., 2017]. We tested three different implementations. The tested three different implementations of DTW, i.e., DTAIDistance [wannesm et al., 2022],

FastDTW [Salvador and Chan, 2007], sktime.distances.dtw_distance [Király et al., 2025] that delivered different results for the same data. FastDTW [Salvador and Chan, 2007] was the fastest, we decided to use the implementation of wannesm et al. [2022] as this is the implementation of the original paper [Berndt and Clifford, 1994], and we could precompute the data before visualization.

4.3.3 HRV metrics

In healthy individuals, the change heart rate (HR) over time is constant and complex, which enables adaptation to environmental and psychological challenges Pham et al. [2021]. Mental health disorders such as depression and cardiovascular disease have been associated with reduced heart rate variability (HRV) Iseger et al. [2020]; Pham et al. [2021] Regarding the time scales, there are three categories of HRV measurements, i.e., long-term (24h), short-term (5 min), ultra-short-term (< 5 min). The results from these three categories are non-interchangeable Shaffer and Ginsberg [2017]. There are three main domains in which HRV is measured, i.e., time domain, frequency domain, and non-linear measures. We use over 80 indices included in the NeuroKit2 package Pham et al. [2021] of these three domains.

4.3.4 Principal Component Analysis

Principal Component Analysis (PCA) [Pearson, 1901] is a dimensionality reduction technique that focuses on maximizing variance and global structures. Another possible dimensionality reduction approach is t-SNE [Maaten and Hinton, 2008]. It is based on pairwise similarities with focus on local structures. We applied PCA on the over 80 computed HRV indices. PCA computes principal components up to the number of initial dimension (HRV indices) and computes how much of the initial dimension contribute to the individual principal components. We used first five or ten most contributing HRV indices to PC1. This enable us to reduce the data but preserve the original axes for further heatmap visualization and clustering.

4.4 T3 Visualization of Results

We design and implement a pipeline for the flexible interaction with the data and the investigation of insights. We visualize the results in order, as domain experts are used to analyzing the data. We start with an overview via heart rate distribution plots, followed by comparisons of runs and blocks using Dynamic Time Warping and clustering heart rate variability metrics.

Based on the research pipeline of domain experts, we visualize the results of comparison methods in three sections. First, we provide a data overview by visualizing the density distribution of the heart rate (Subsection 4.4.2). Domain experts prefer to first look into the data HR in the full length and compare the runs. Second, we therefore visualize

the comparison over different run types (Subsection 4.4.3). Third, we visualize the comparison of blocks (Subsection 4.4.4).

4.4.1 Implementation

As we built the visual analysis pipeline for research in the early stages, we decided to implement the framework in Jupyter notebooks. It enables more flexibility and adaptation. Through Python scripts, we implemented the core functionality. We implemented separate Jupyter notebooks for data pre-processing, automated data analysis, and results visualization. The domain experts were used to working with scripts in programming languages in their previous approach, which enables the use of Jupyter Notebooks as a user interface. The main advantage of this approach is that it allows for easy integration into a larger processing pipeline, possibly with other modalities, flexibility, and modifications for future data and research.

4.4.2 Data Overview

To provide an overview of the data, we use kernel density estimate (KDE) plot. KDE visualizes the data distribution similarly to a histogram. In contrast to the histogram, the KDE plots are represented by a line, which makes them suitable for comparison of different density distributions. We use KDE to visualize the whole measurement distribution and the individual blocks' distributions. This gives a general overview of initial data inspection and identifies subjects with unexpected distribution, indicating errors in the data. For visualizing the KDE diagram we used the HSLuv cyclic color palette. The HSLuv palette in seaborn enables more than 8 colors.

Figure 4.10 shows the KDE plot of blocks from each run for subject 01. Peaks represent the most frequently represented HR values. Different line styles are used for the three block types. For the majority of the blocks, the peak was around 20, whereas for block 3 of the run resting state, the highest peak was around 95.

4.4.3 Comparison of Runs

To measure the similarity of runs, we use DTW pair-wise on runs per subject, visualized with a scatterplot. An example of dtw plot is visible in Figure 4.12. To measure the difference in heart rate variability using over 80 heart rate variability indices. PCA is applied to reduce the dimension within the heatmap or the clustermap visualization. Heatmap preserves the order of rows, whereas cluster changes the order of rows to group the most similar. Figure 4.11 shows a clustermap of subjects for different runs that form two different clusters.

4.4.4 Comparison of Blocks

We use a scatterplot to visualize distances using DTW between blocks within a subject. We use a colorblind palette to visualize different pairs of blocks. Figure 4.12 shows such a

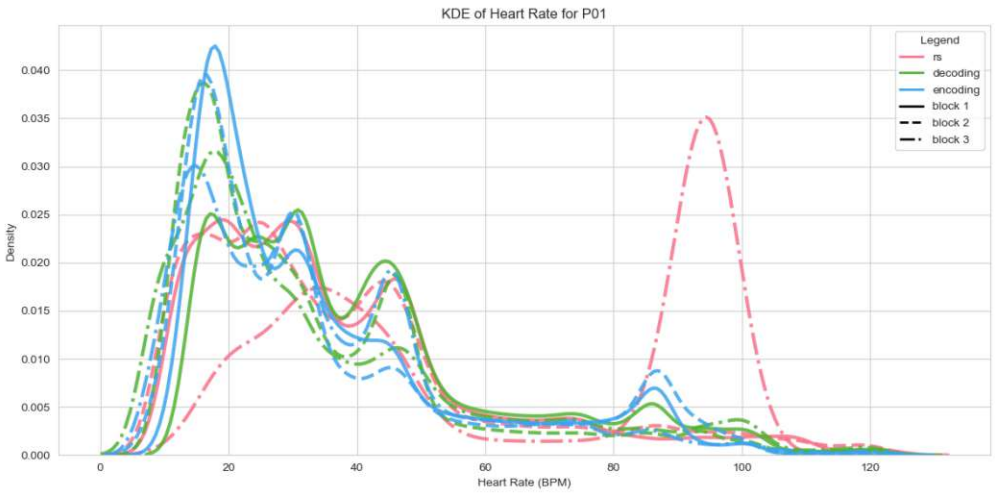

Figure 4.10: An example of KDE plot of subject 1 with color encoding of different runs using HSLuv palette and line style representing different blocks.

scatterplot. In addition, we used markers to visualize different runs. The number of blocks was too overwhelming. Therefore, we use a clustermap instead of a heatmap. Clustermap combines a heatmap with dendrogram clustering. An example of the clustermap is visible in Figure 4.11.

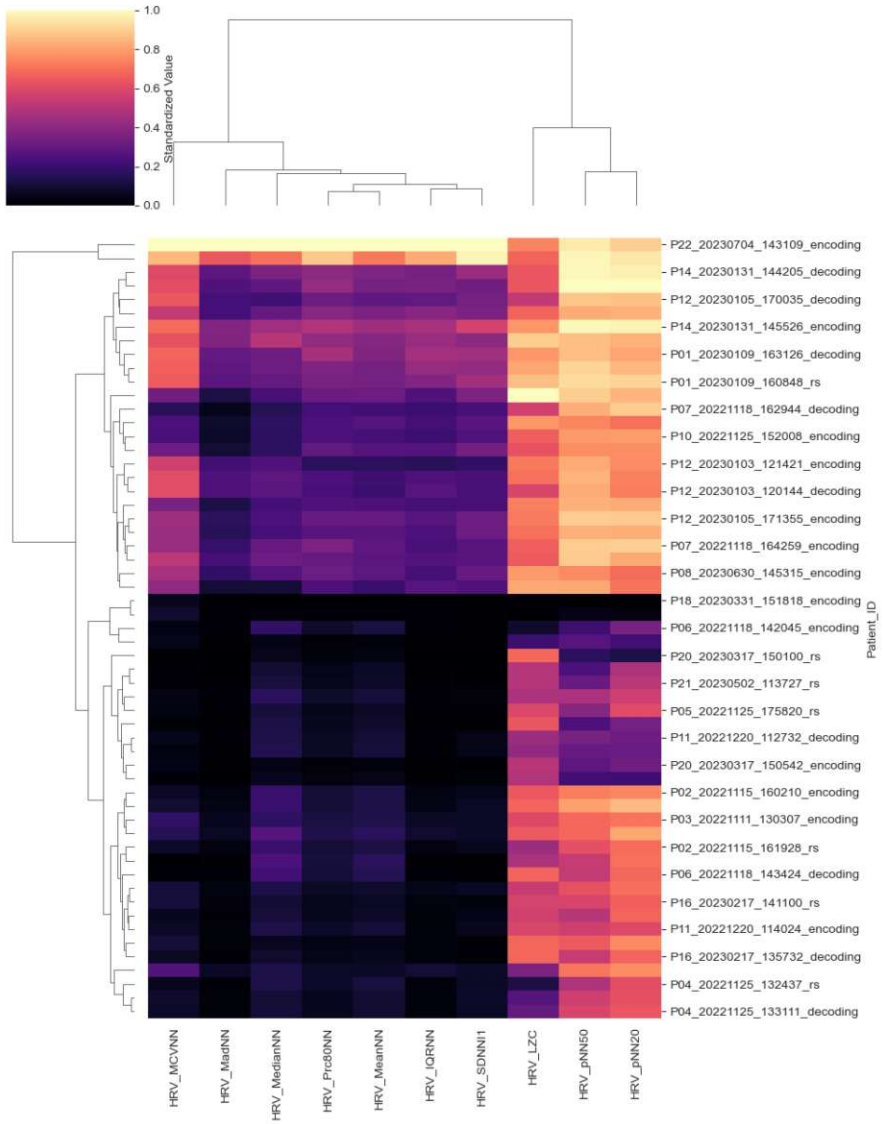

Figure 4.11: An example of clustermap for comparison of different runs using magma color palette.

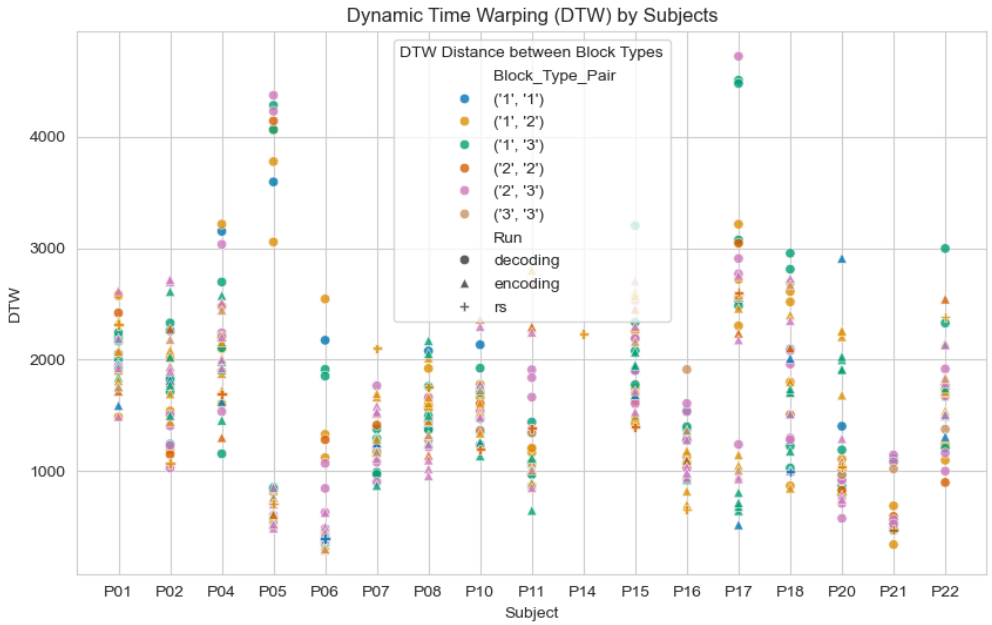

Figure 4.12: An example of a scatterplot with DTW similarity scores for block similarity within subjects. Markers encode the run type.

CHAPTER 5

Results

In this chapter, we present results of different steps of our visual analysis pipeline. We designed and tested automated pre-processing and processing techniques on generated data to support the workflow of domain experts in their data analysis. In section 5.1 we present quantitative results of automated analysis on generated ECG data. We designed a visual analysis pipeline and proposed a walkthrough Isenberg et al. [2013], where we demonstrate possible usage scenarios of how domain experts could use our visual analysis pipeline. The walkthrough is presented in section 5.2, where we provide Qualitative Result Inspection (QRI) Isenberg et al. [2013]. QRI was introduced by Isenberg et al. [2013], where the viewer is involved into the process of qualitative evaluation by assessing the resulting images.

5.1 Quantitative Results of the Generated Data

In this section, we present quantitative results of different imputation and noise reduction techniques measured for generated data.

5.1.1 Missing Data: Imputations

We compared different imputation approaches. The best results were obtained with linear and polynomial interpolation. Figure 5.1 shows the imputed values for linear and polynomial interpolation were very close to a perfect match. This corresponds to the findings of Steffen et al. Steffen et al. [2015]. Figure 5.2 shows the metric values for the imputation method that were close to zero for linear and polynomial interpolation. For the highest deletion rate of 0.2, the highest were the RMSE values with values to the power of -3 for linear interpolation and -5 for polynomial interpolation. LOCF and NOCB had RMSE values around 0.015. We decided to use linear interpolation as an imputation method for the measured data, even though it has slightly lower results than

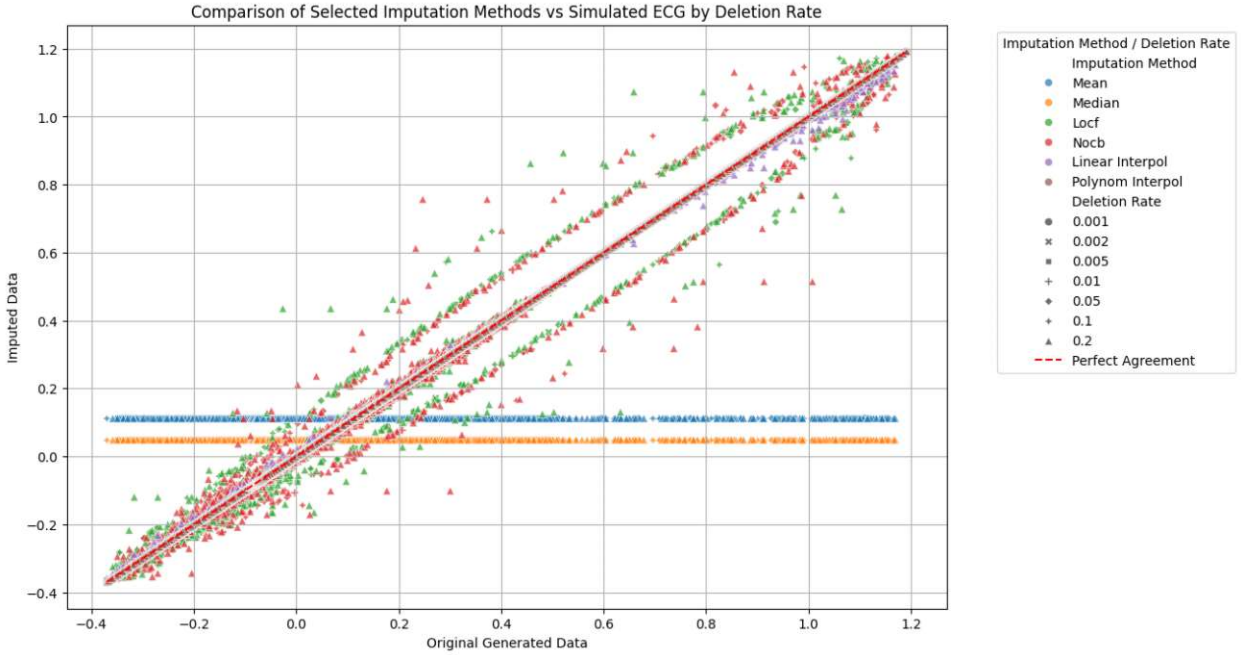

Figure 5.1: Scatterplot visualizing the imputed values (y-axis) vs generated data. As expected, mean and median imputations have constant values regardless of the values of the generated data. LOCF and NOCB imputed values were around perfect agreement, with increased distance with increasing deletion rate. Linear and polynomial interpolation as an imputation method are very close to perfect agreement.

polynomial interpolation. If performance is the high priority apart from accuracy, LOCF and NOCB perform quite well, especially with a lower amount of missing data. These results are for the generated ECG data with a frequency of 400 Hz.

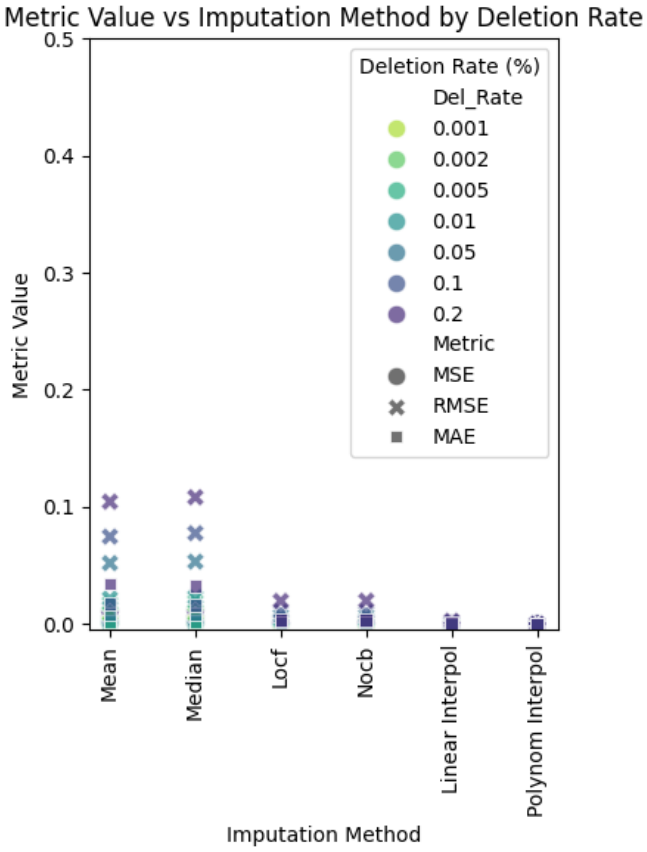

Figure 5.2: MSE, RMSE, MAE of different imputation methods, where linear and polynomial interpolation have the lowest metric values even for high deletion rates.

5.1.2 Noise Reduction

We tested six approaches to reduce noise. The most accurate was the neurokit2 high-pass butterworth filter implementation Makowski et al. [2021]. Both neurokit2 and biosppy Bota et al. [2024] implementation have MSE, MAE values under 0.5 and signal-to-noise ratio around 10. All approaches had similar accuracy for all noise types (Figure 5.3). These results suggest that filters from general signal processing with fine-tuning on ECG data perform better as approaches focusing on QRS features.

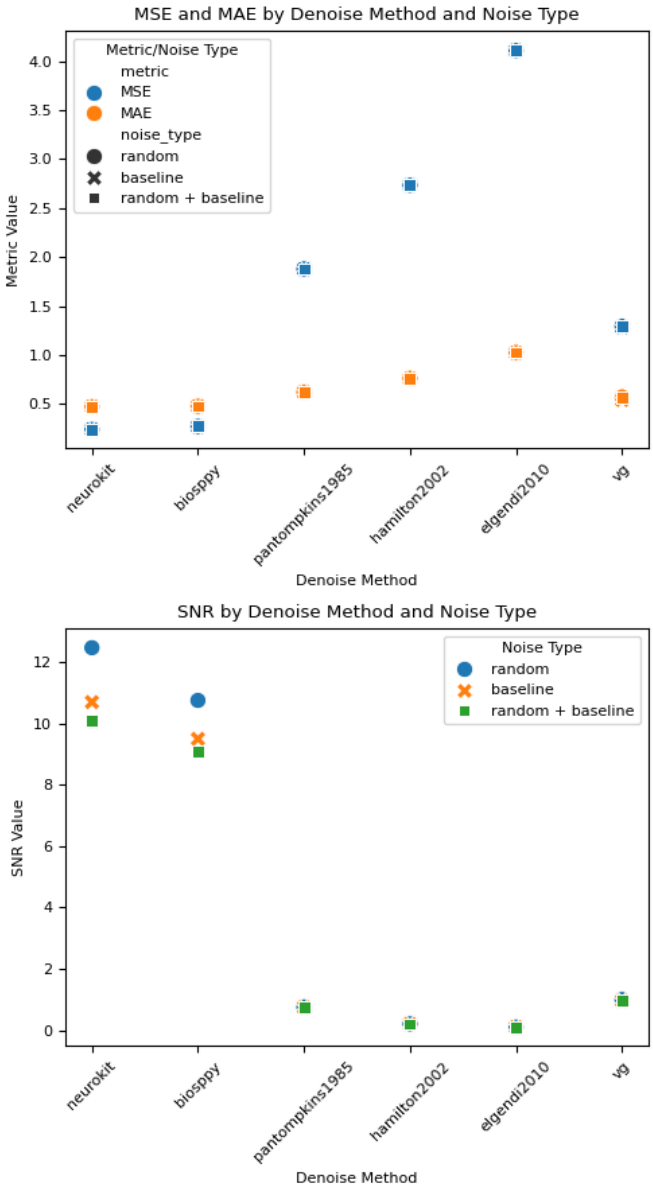

Figure 5.3: Comparison of noise reduction methods. (TOP) MSE, MAE metrics, (BOTTOM) signal-to-noise ratio. The lowest metric values and the highest signal-to-noise ratio.

5.1.3 HRV Metrics and Generated Data Comparisons

Out of the comparison reasons for the measured data, we applied the comparison methods to the generated data. As domain experts are used to starting with a statistical test to measure a significant difference, we measured statistical significance. We tested the data

for normality using the D'Agostino-Pearson test D'Agostino and Pearson [1973]. As we used pairwise comparisons, we used the Mann-Whitney test. The results were almost always near 0. This indicates that the data themselves differ over time even without changing the parameter.

We applied the different HRV metrics to generated data with different HR simulations. Figure 5.4 shows the clustermap of the top 10 most contributing HRV metrics to variance

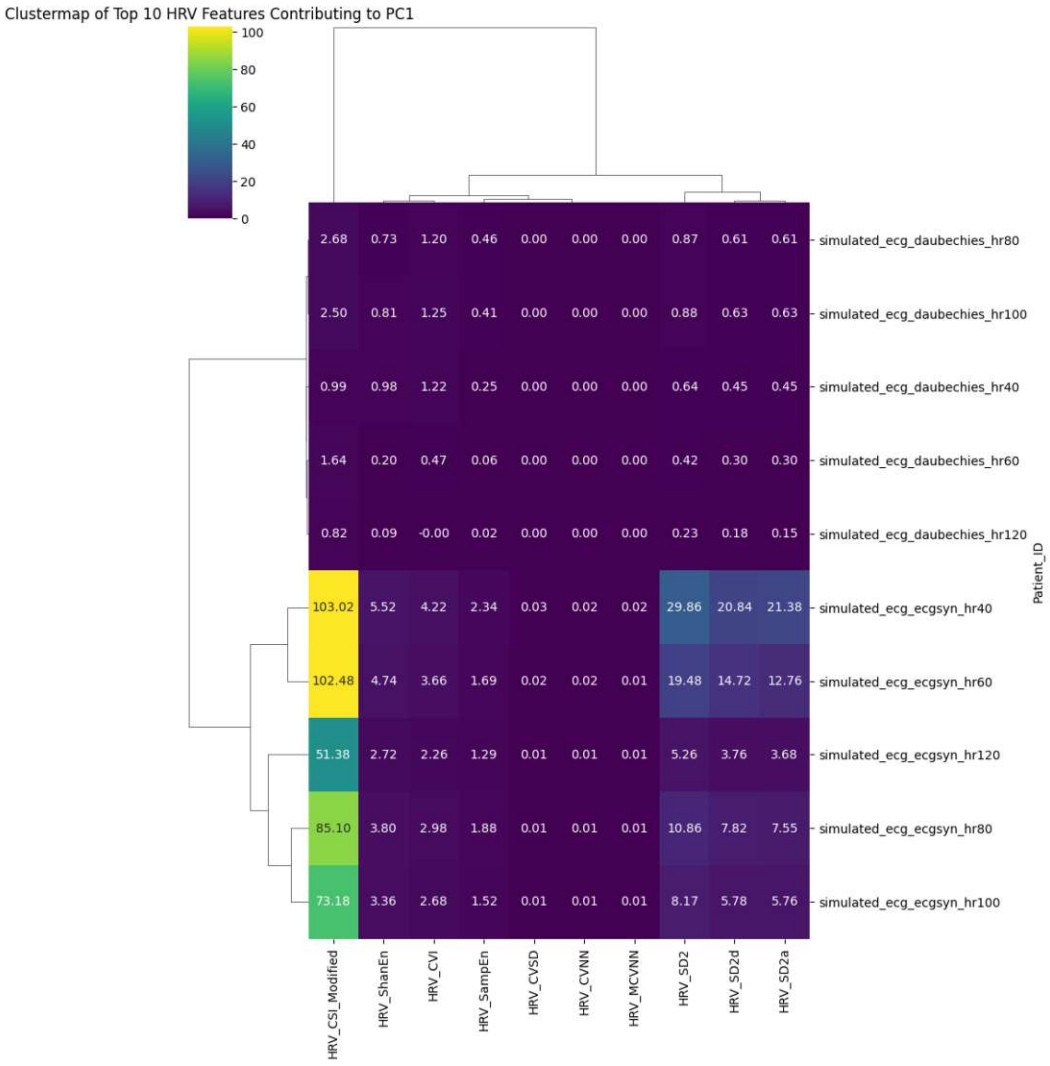

(a) Clustermap with HRV metrics of simulated subjects without data normalization

Figure 5.4: Clustermap contains HRV computed from simulated ECG with 2 different simulation methods, i.e., ECGSYN and Daubechies, and different HR. Simulated subjects are clustered by 10 HRV selected by PCA. Slight changes in the resulting cluster are visible depending on whether normalization is used (a) or not (b).

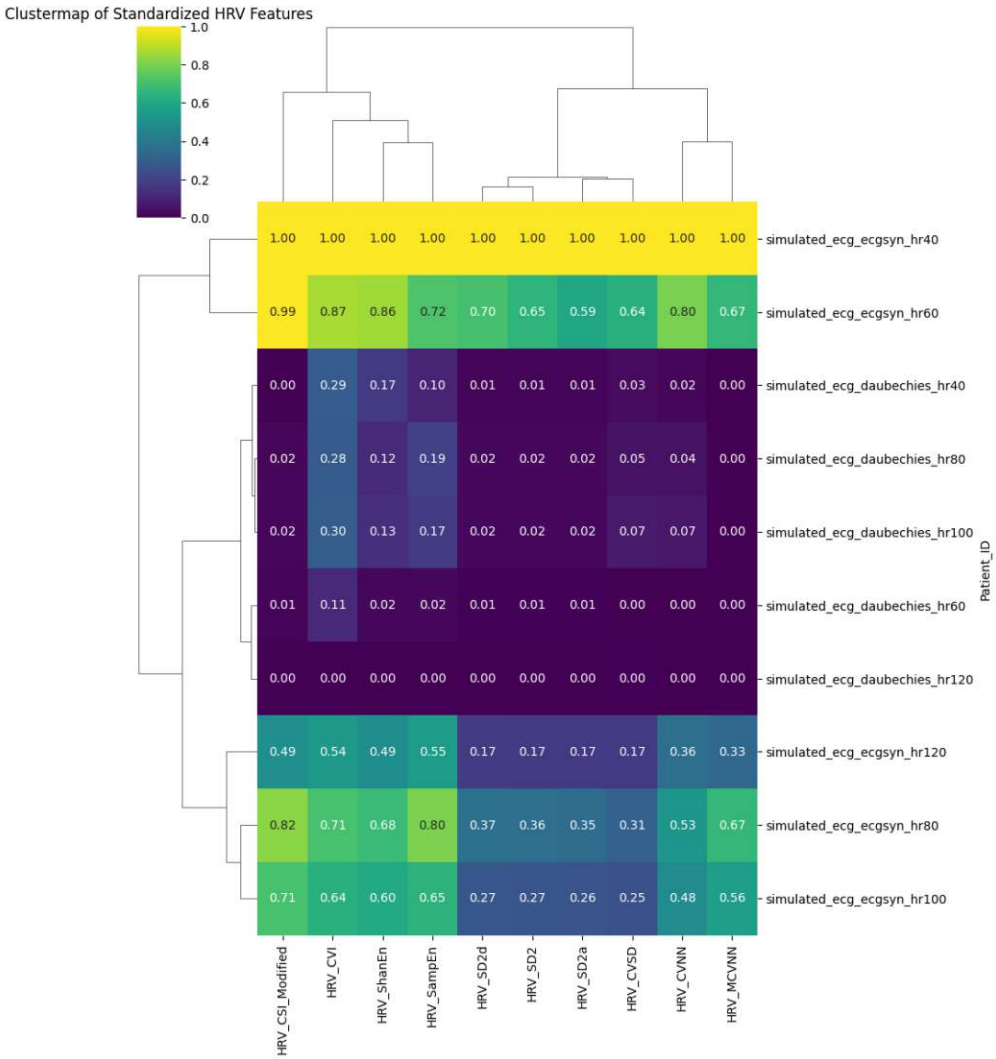

(b) Clustermap with HRV metrics of simulated subjects with data normalization

Figure 5.4: Clustermap contains HRV computed from simulated ECG with 2 different simulation methods, i.e., ECGSYN and Daubechies, and different HR. Simulated subjects are clustered by 10 HRV selected by PCA. Slight changes in the resulting cluster are visible depending on whether normalization is used (a) or not (b).

in the data. There is a slight difference in dendrogram cluster formation depending on whether normalization is used (Figure 5.4b) or not (Figure 5.4a). The Daubechies had generally very low HRV values. It was expected, as this method of generating ECG data is very regular. ECGSYN tries to simulate real-world variability in the data. The Daubechies method was clustered together both with and without normalization (Figure 5.4). Whereas when normalized data were used for clustering, ECG was divided into two

clusters, one for lower and the other for higher HR.

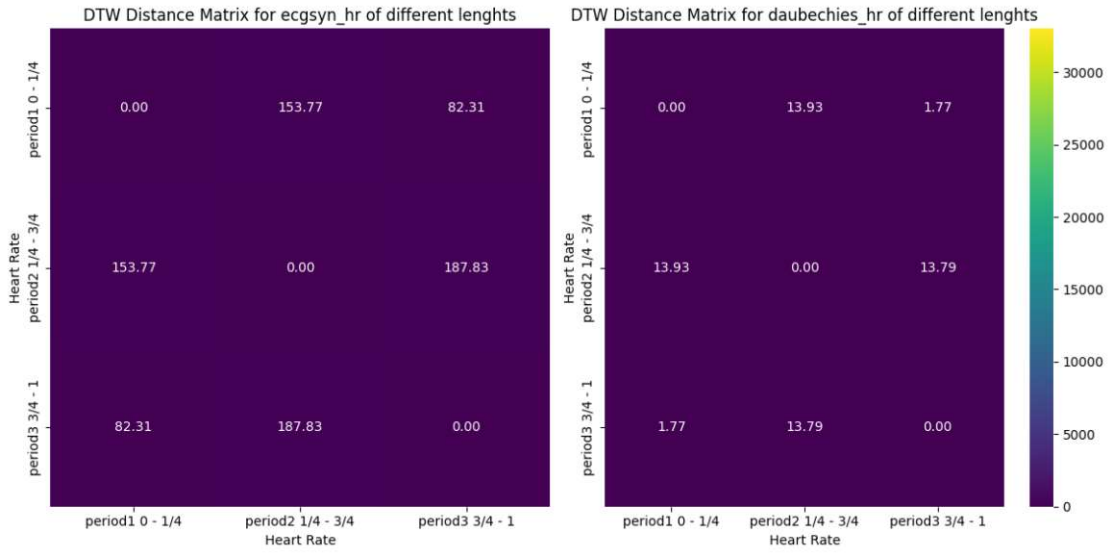

(a) DTW similarity scores for generate ECG data of different lenghts.

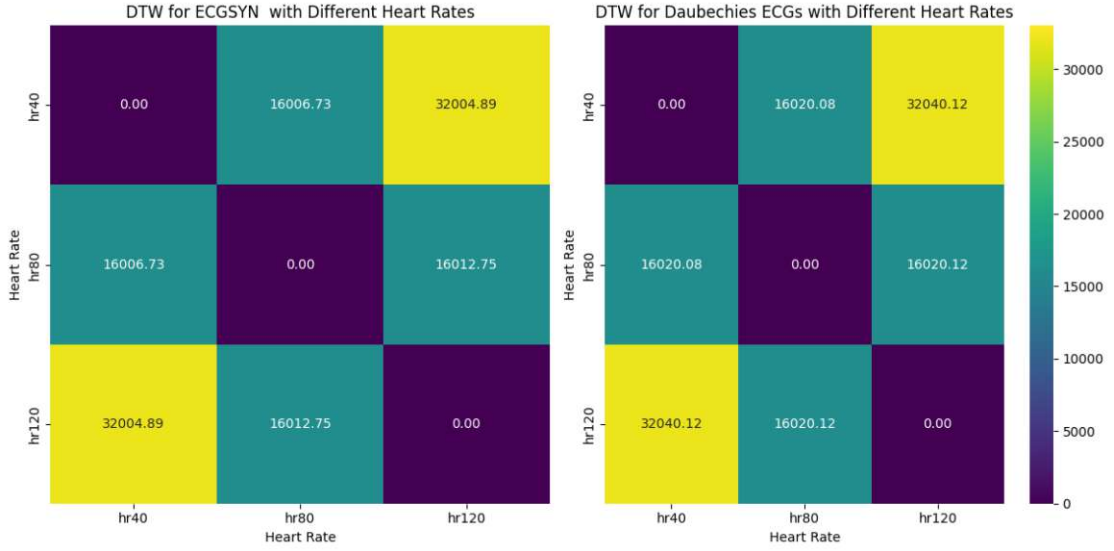

(b) DTW similarity scores for generate ECG data of different HR.

Figure 5.5: Confusion matrices of DTW similarity scores of (a) different length and (b) different HR values. On the left, there are ECGSYN-generated data, and on the right, there Daubechies Daubechies-generated ECG data. The same scale is used for both Figures, indicating minimal difference based on the length difference of two ECG signals, yet a significant increase with increasing HR difference.

In the synthesized data, we tested how the different heart rates (Figure 5.5b) and different

lengths (Figure 5.5a) of the data influence the DTW similarity scores. DTW matrices (Figure 5.5) show that with increasing HR values, the scores increase significantly, whereas for the data of different lengths the DTW distance between the data was minimal. It corresponds to findings of Ratanamahatana and Keogh [2005]. This indicates the DTW is suitable for measuring the difference in HR in two subjects.

5.2 Qualitative Result Inspection

We observed and discussed with domain experts their research workflow. Based on that, in this section we describe some of our framework's possible usage scenarios and provide Qualitative Result Inspection (QRI).

5.2.1 Interactive Preprocessing

We enable the user to choose missing data handeling method and noise reduction method. We visualize the data to support decision making of appropriate pre-processing steps. Visualizing the input and output of the pre-processing together supports the fine-tuning of parameters, e.g., for noise reduction Bernard et al. [2012].

5.2.2 Data overview using KDE plot

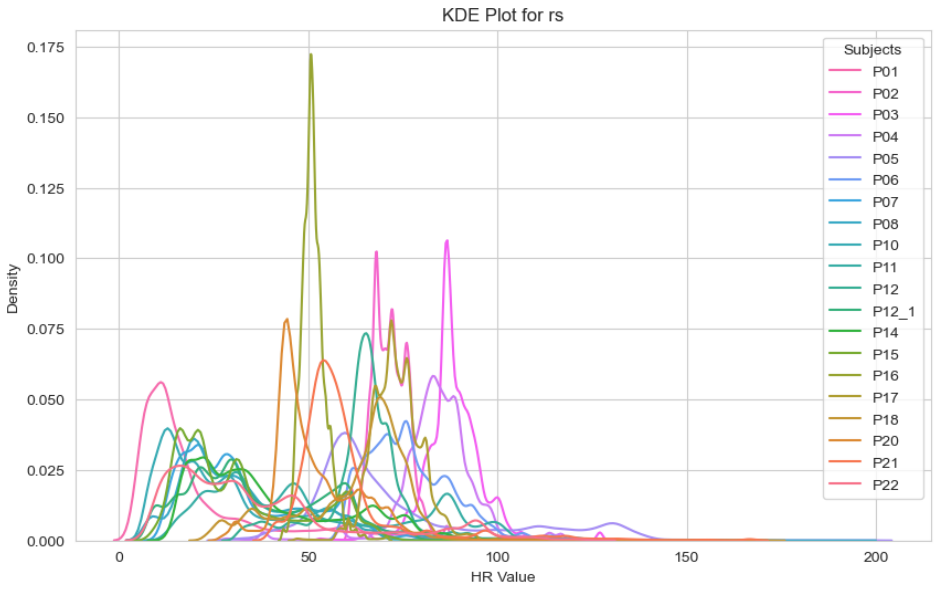

(a) KDE plot for all subjects of the run resting state showing their distribution.

Figure 5.6: KDE plot representing the distribution of HR at different levels of granularity.

Kernel density estimate (KDE) plot visualized the distribution of heart rate (HR). Domain experts can acquire a brief overview of the data and identify subjects with unexpected

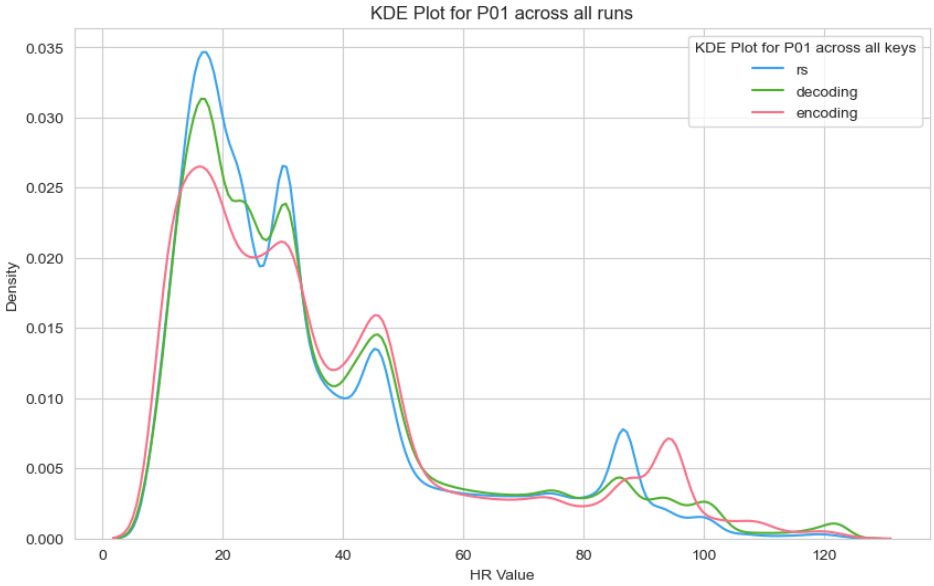

(b) KDE plot of subject 01 showing very similar distribution of HR values for all three runs.

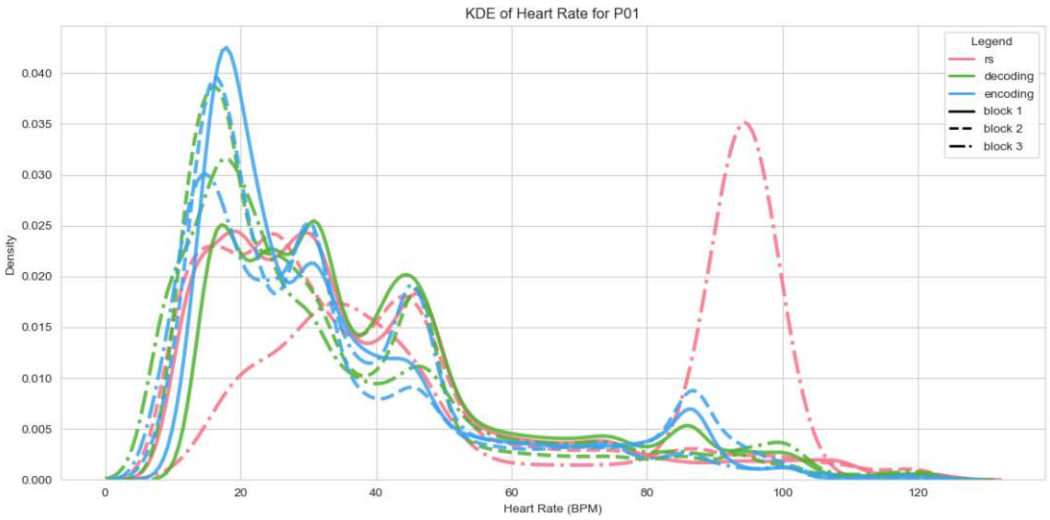

(c) KDE plot of one subject HR divided into blocks over all runs.

Figure 5.6: KDE plot representing the distribution of HR at different levels of granularity.

distributions, mainly too low or too high, that could indicate some errors in the data. The user can select a subject to compare distributions in different runs and blocks. In addition, the user can select a run to compare the variability of the distribution of HR of different subjects. Figure 5.6 shows the KDE plots in different levels of granularity. In Figure 5.6a show the peaks of the data distribution are spread throughout the values

from 0 to 100 for different subjects in the resting state, whereas the distributions across run types for subject 1 were very similar (Figure 5.6b) low values, only block 3 in resting state had a higher peak (Figure 5.6c).

5.2.3 Using DTW to Measure Pairwise Distances between Runs

We present a scatterplot (Figure 5.7) to examine the similarity of the heart rate (HR) over time across various runs. Domain experts can use to investigate intra-subject variability or to compare HR of different runs within a subject.

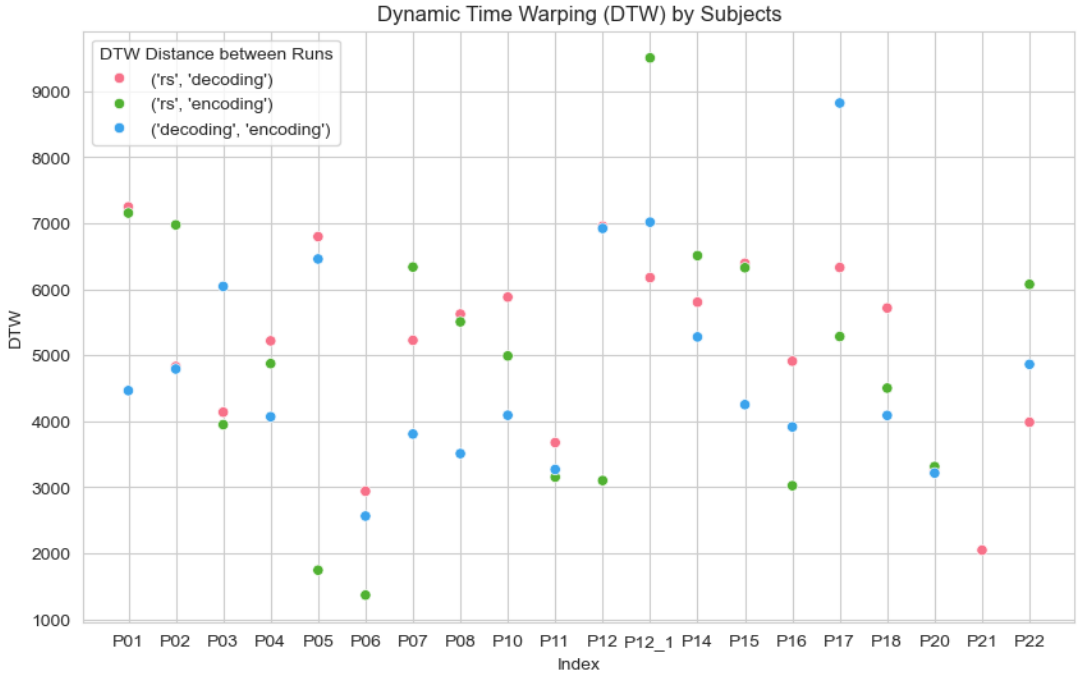

Figure 5.7: Dynamic Time Warping for run comparison within subjects.

In Figure 5.7, the data appears to be widely distributed. Most subjects distance between 3000 to 7500. Some subjects have very low DTW values, such as subjects 5, 6, and 21. Others have one higher score, i.e., subjects 12_1 and subjects 17. For subject 12, there was more than one measurement; we always computed between pairs, but this should be further evaluated by domain experts.

5.2.4 Inspect HRV Metrics over Duration of Session to Compare Runs

To observe change in the heart rate, domain experts can inspect different heart rate variability (HRV) metrics through a heatmap (Figure 5.8). Of the more than 80, the user chooses the selected metrics manually or by Principal Component Analysis (PCA). The user can choose to perform PCA only on a selected run or on all runs together. These heatmaps can be used to, e.g., compare different runs and indicate patterns in the data. For more details, the dataframe with exact values can be filtered according to preference. Subject 22 had the highest values for encoding and decoding, for the resting state, too many HRV indices contained NaN values, and the HRV data were therefore excluded from further PCA steps and heatmap visualization. Further investigation by domain experts is required for this subject. Subject 7 - 15 has higher values than subjects 2 - 6, 11, and 16 - 21. The given HRV indices characterize these two clusters.

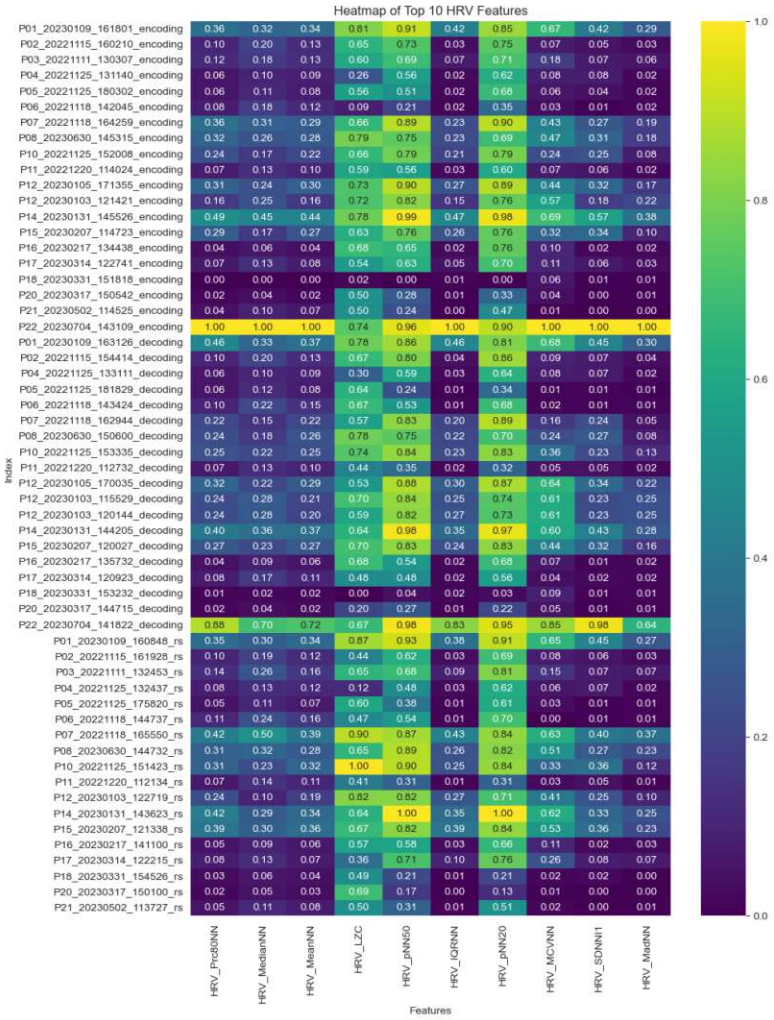

Figure 5.8: Heatmap with heart rate variability for run comparison.

5.2.5 Using DTW to Measure Pairwise Distances between Blocks

Within our framework, it is possible to visualize all distances between different block combinations (Figure 5.9). It enables observation of outliers within the data. The user can also filter block pairs to be visualized and inspect whether similar patterns occur in all runs. It is also possible to filter only certain runs that should be included in the visualization. By default, we visualize the distances between block 1 vs block 3 and block 2 vs block 3, as the main focus of domain experts is to compare block with and without TMS impulses. For additional information, including the precise start and end times of concrete blocks, we include a dataframe that supports filtering and reordering of columns.

In Figure 5.9, Block 3 without TMS impulses was selected in pairs with block 1 and 2, where TMS is present. In both Figures 5.9 some subjects such as subject P05 or P17 either relatively high distances for the decoding run or very low distances. Other subjects such as P01, P02, P11, P15, P18 were more spread out in the middle with DTW scores around 1000 to 3000. These scores are generally lower than the differences between simulated data with different HR.

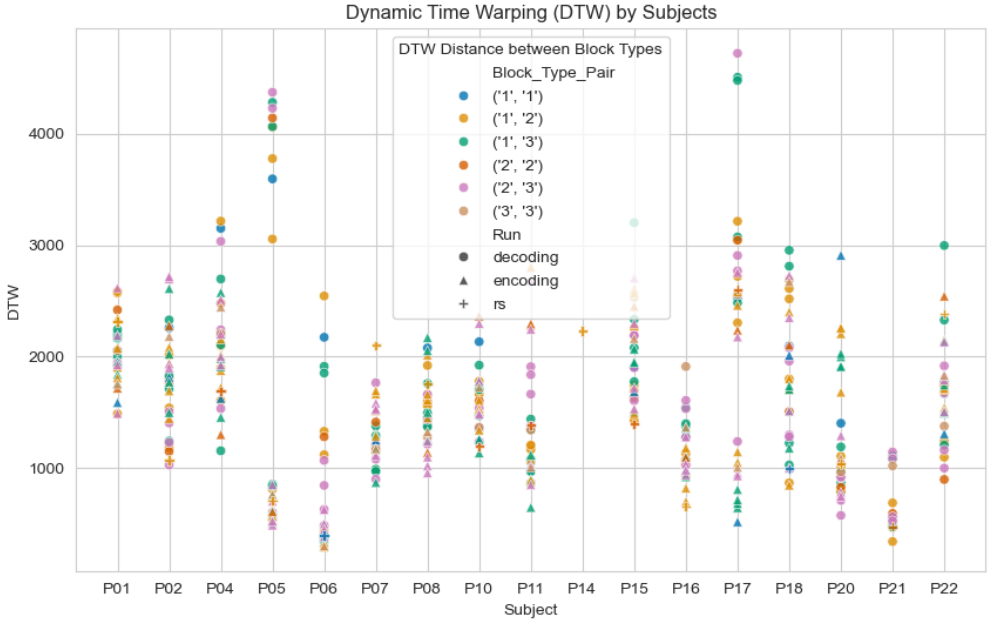

(a) DTW for all possible block types comparisons.

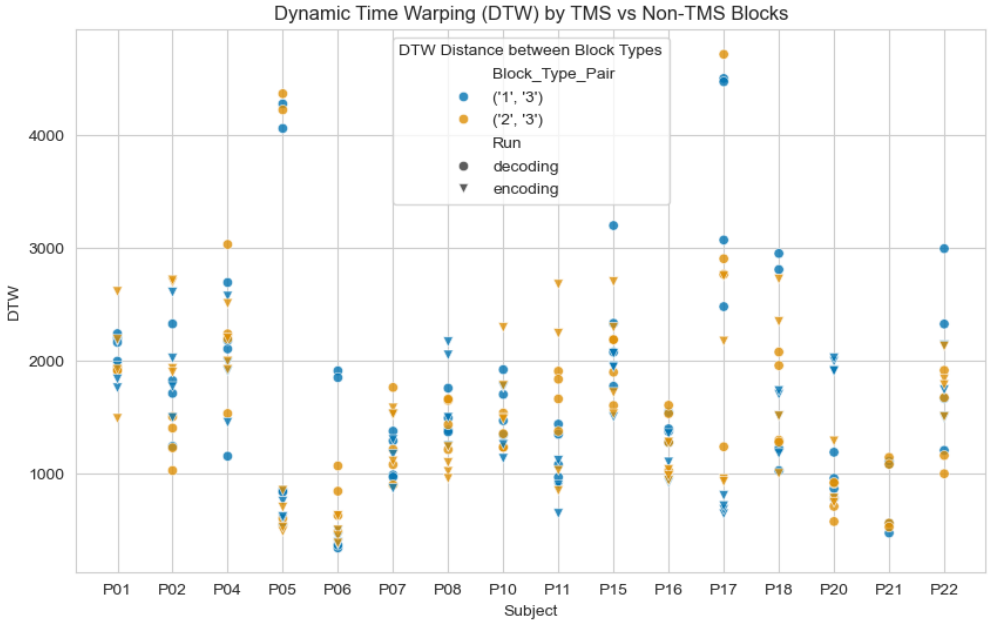

(b) DTW with user-selected block types comparisons.

Figure 5.9: Scatterplot of DTW for block type comparison. Runs, i.e., decoding, encoding, and resting state (rs) are distinguished by markers.

5.2.6 Clustering HRV Metrics over Block

Automated heart rate variability (HRV) metrics were calculated for every block of ECG data. To find patterns and in the data, we provide a clustermap that combines a dendrogram with a heatmap (Figure 5.10). By default, PCA is utilized to filter HRV metrics, though manual selection is available as well. users can choose whether to used normalized data or the exact HRV values. In addition, domain experts can choose to visualize certain parameters of interest such as block type or run type.

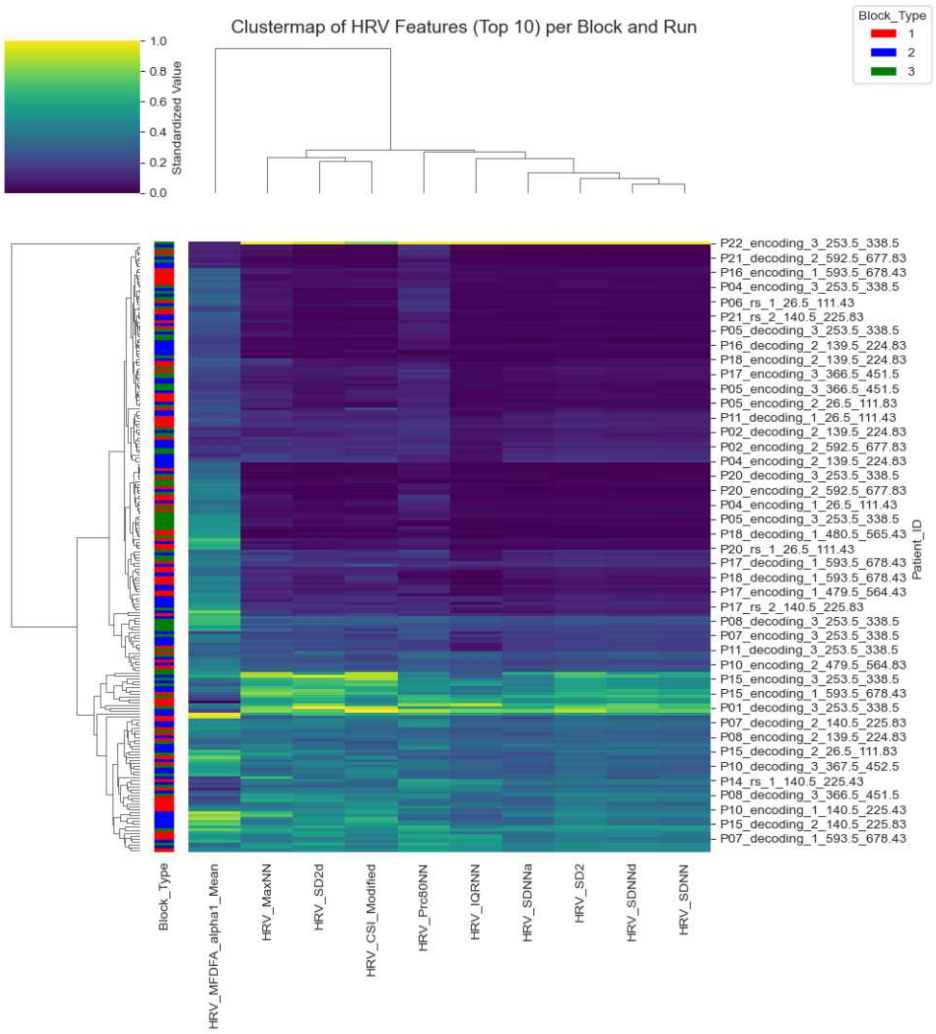

(a) Clustermap with run block type visualization.

Figure 5.10: Clustermaps of top 10 HRV metrics contributing to difference in the data computed from block time sequencies of ECG data.

Three dominant clusters. The one with the highest values consists of subject 22. In the context of the HRV for the entire ECG sequence from various runs, this could indicate

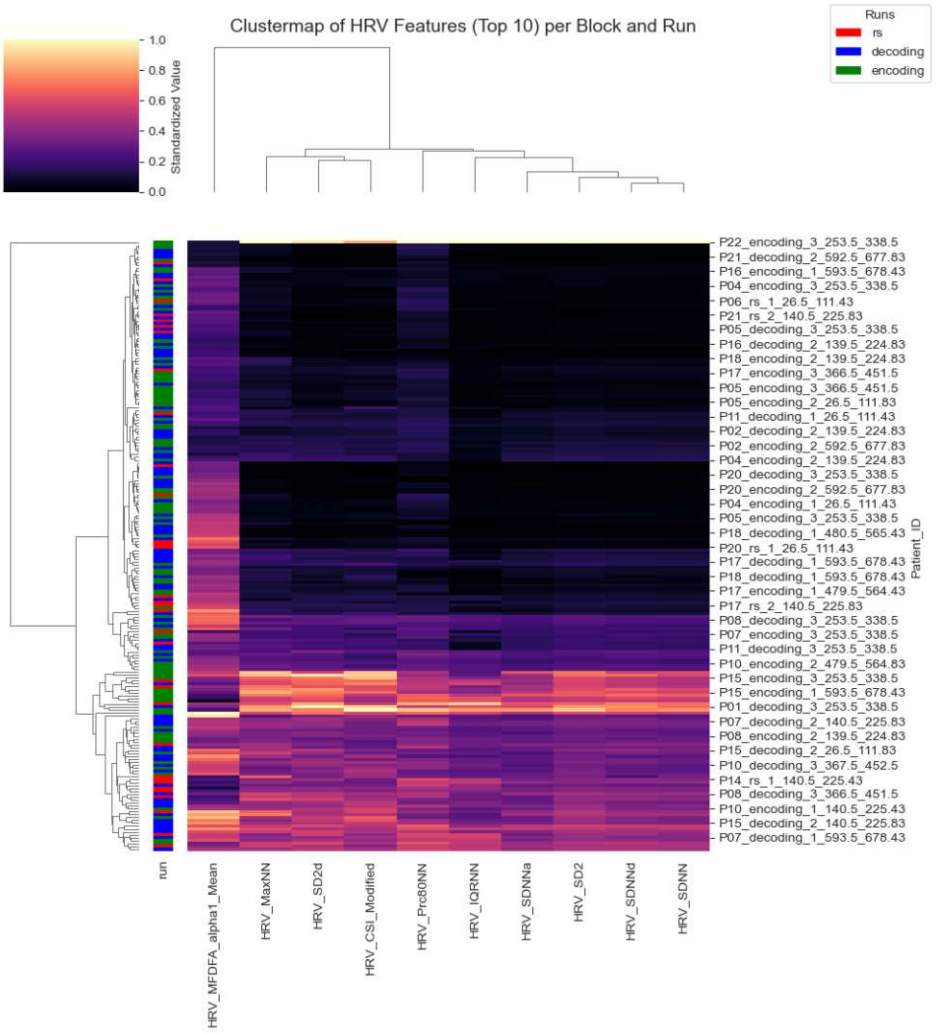

(b) Clustermap with run type visualization.

Figure 5.10: Clustermaps of top 10 HRV metrics contributing to difference in the data computed from block time sequencies of ECG data. These clustermaps can be visualized with different data properties such as (a) block type, and (b) run type.

that the data are incomplete, but further inspections should be accomplished to determine this separate cluster. From the other two, one has higher numbers than the other. With the different HRV indices, these clusters can be characterized.

5.2.7 Printing Results

Although computer-based visual analytics framework gives many possibilities to explore data, find patterns, and define hypotheses, in the creative process of early-stage research

often helps to have a paper and pen. As a part of our visual analysis pipeline, we provide users with the possibility to export the PDF of the different stages of the pipeline. PDF can be exported from different parameter settings of the same step or different steps.

5.3 Quality Criterion

Expressiveness

Visual inspection and quantitative evaluation allow users to determine the impact of the pre-processing steps on the ECG data. Lineplots (e.g. those in Figure 5.6) allow for visual inspection of the effects of noise reduction techniques. Clustermaps enable easy distinction of different subgroups of data and characterize them. DTW shows the distances in the data that support determining whether the distances between certain criteria, such as blocks and runs, are larger than the distances within these subgroups. In this way, the expressiveness criterion by Miksch and Aigner is met.

Appropriateness

We have built a visual analysis pipeline that allows users to easily differentiate and characterize subgroups of data by clustering HRV and allows users to see the difference in the data by DTW. This simple solution does not overwhelm users, instead, it supports users in gaining insights from the data. Furthermore, we support not only the human vision but also cognitive capabilities related to the application domain by allowing users to customize the pipeline. Thus, we fulfill the appropriateness criterion set by Miksch and Aigner.

Effectiveness

Density distribution plots and clustermaps are known in the application domain. With KDE plots, users gain a general overview of the data. It enables users to determine possible outliers or an unexpected range of HR values in the data that require further investigation. With clustermaps, users can characterize the cluster with HRV metrics. DTW enables comparison of different time periods of HR data and visual exploration of possible patterns. These approaches enable users to interact with data effectively. In this way, the effectiveness criterion established by Miksch and Aigner is satisfied.

Integrability

To make the visual analysis pipeline integrable, we considered a previous research workflow in the domain. To ease users' adaptability, we combine the basic approaches, namely statistical approaches with automated and visual analysis. General overview of the data distribution used to be the first step of the analysis pipeline in the previous research workflow. To ensure the tasks' compatibility, we provide a general overview of the data distribution using the KDE plot and extend the data exploration by characterizing

clusters of data based on HRV metrics and data comparison by providing DTW distance scores. We maintained the legacy of the data by converting the data to a compatible data format and respecting the blocks the TMS were divided into, i.e., blocks with and without TMS impulses. Thus, we satisfy the fourth integrability criterion, which that we introduced.

5.4 Discussion and Limitations

By introducing Data–Users–Workflow-Tasks design pyramid, an extension of D-U-T triangle [Miksch and Aigner, 2014], we provide a new perspective on designing a visual analysis framework for early-staged research. We propose considering the previous workflow, especially for cases, where the data processing workflow in the application domain has not yet been well established. In our case, the tasks were defined only on a very high level, i.e., as general hypotheses in the research domain. Yet, the low-level tasks definition necessary for implementation was missing, the data had been derived from previous research, and the users were not sure how they would analyze the data. We extended the previous workflow of brain stimulation researchers by designing a visual analysis pipeline for ECG and TMS data processing to allow data pre-processing and visual data exploration and comparisons. In this section, we discuss the applications and limitations of our visual analysis pipeline for the NCG-TMS domain.

Handling Missing Data in ECG Signal Our visual analysis pipeline starts with data extraction and pre-processing. To support the decision-making process of choosing a missing data handling approach, we conducted Little's MCAR test and computed the amount of missing data. To evaluate imputation methods, we used simulated single-lead ECG data. In the measured data, the missingness occurs at the level of the raw electrode signals. We used the same sampling frequency of 400 Hz for the simulated data as it was used in the measured data. As ECG leads are computed as a difference of electrodes, the minimal necessary number of electrodes for ECG is two. In our case, the ECG data were acquired by four electrodes. This makes the raw electrode signals multivariate time series even in case of a single-lead ECG. The results of simulated data show the best accuracy with RMSE values as low as to the power of -3 and -5, respectively, for linear and polynomial interpolation (Figure 5.2), which we used as univariate imputation methods. Based on these results, we hypothesize that the ECG acquisition with sampling frequency of 400 Hz contains redundancy and that the information remains in the data even after 20% of randomly deleted data. We assume that the data redundancy is not changed by the process of ECG lead extraction, namely the time series subtraction. Therefore, we assume linear and polynomial interpolation as univariate imputation methods are also suitable for handling the missingness in multivariate electrode signals.

ECG Noise Suppression For the NCG-TMS application, as HR is of interest, the most crucial part is to identify R-peaks correctly. If noise interferes with the R-peaks, this could directly influence the HR and its further analysis Iseger et al. [2021].

We evaluated the denoising techniques on the two most common noise sources, i.e., baseline wander and power-line interference, that have been defined in the literature and can be added to the clean signal [Singh et al., 2019], respectively, in our case, simulated ECG. The measured data we worked with in this thesis were acquired during fMRI imaging in a fMRI induced magnetic field [Grosshagauer et al., 2024]. Many of the papers on ECG denoising [Chatterjee et al., 2020; Elgendi et al., 2010; Hamilton, 2002; Joshi et al., 2013; Kher, 2019; Mir and Singh, 2021; Pan and Tompkins, 1985; Singh et al., 2019] do not work with data acquired in a magnetic field. Studies that work with MRI induced noise removal require acquiring magnetic field gradient [Oster et al., 2010] or use hardware-based noise removal [Laudon et al., 1998]. If other noise sources, such as magnetic field interference, were to be identified and defined by domain experts, our noise reduction evaluation pipeline can be applied to these other possible noise sources as well. Within our visual analysis pipeline, domain experts can use it to visualize raw ECG leads and the denoised ECG signal to inspect the effects of different noise removal techniques visually.

Comparisons and Data Exploration As domain experts were used to working with statistical tests to correlate data, we applied the Mann-Whitney test, a non-parametric statistical test, to both generate and measure data, based on our results that both simulated and measured ECG data were not normally distributed. The results were almost always near zero. It indicates HR varies strongly over time even without changing the state of the subject (resting state vs. task) or applying TMS impulses. This corresponds to literature findings that in healthy subjects there is a variability in HR over time [Pham et al., 2021]. We therefore excluded this approach from further steps of the visual analysis pipeline, i.e., visualization.

We compute over 80 HRV metrics [Frasch, 2022] for two different time lengths to support data investigation. The use of the duration of one measurement session and the division of the data into individual blocks were named by domain experts as a good start for data investigation. Some HRV metrics were not computed especially for the blocks as they would need longer time periods. The computed metrics can be used to characterize and study the heart rate variability in these two time lengths. If other periods of interest were to be defined in the future, they could be integrated into our visual analysis pipeline with slight changes. Using PCA, we identify the metrics with the most difference in data and visualize the selected metrics in a clustermap. Users can also select the metrics of interest manually. The clustermap visualizes the dendrogram clustering. The resulting cluster can be further explored for characteristics. Additional data properties can be visualized alongside the data to investigate patterns in the data. In the simulated data, the clustering results slightly differed when using normalized data and without normalization (Figure 5.4). In both cases, the Daubechies simulated ECG was clustered together, but in clustermap with the normalized data, the ECGSYN simulation was divided into two separate clusters, one with low heart rate and one with higher heart rate values.

To provide a comparison of how similar or distant two heart rate sequences are, we computed DTW scores. In the measured data, we applied the DTW to the whole session duration and block division as suggested by domain experts. With slight updates, other time periods could be compared within our visual analysis pipeline. We visualize the scores in a scatterplot to compare the DTW scores across subjects. The simulated data show an increase in Dynamic Time Warping (DTW) scores with increasing HR difference.

Hypothesis Testing As we designed and implemented our visual analysis pipeline for early-stage research, our primary focus was on data exploration. During the time period of conducting this thesis, the concrete application domain hypotheses had not yet been formulated. Only the abstract domain hypotheses described in Subsection 2.5.3 were available, i.e., state-dependency of TMS effects, and HR deceleration as a result of TMS. As a starting point for testing these hypotheses for the current data acquisition settings, domain experts suggested comparing the entire sessions across different runs to evaluate state dependency and the comparison of blocks to evaluate HR decrease after TMS stimulation. Our visual analysis pipeline enables visualization of parameters such as run type or block type alongside the clustermap with HRV metrics to determine whether these data characteristics are clustered together. This was not the case in our measured data, both the run types and block types were spread throughout the clusters (Figure 5.10). Furthermore, we use DTW to determine the similarity of two given time series. Our results in this manner are inconclusive and suggest more complex relations in the data.

Our visual analysis pipeline can give insight into future hypothesis formulations, especially if these were connected to experimenting with different lengths of time periods. Based on the concrete formulation of the low-level hypothesis, other visual analytics approaches might be necessary to complete the hypothesis testing.

Generalization od D-U-W-T pyramid We extended the Data–Users–Tasks design triangle by considering also previous research workflow within the design of the visual analysis pipeline to support early-stage research of TMS and ECG data. This extended D-U-T triangle, namely Data–Users–Workflow-Tasks design pyramid, could be generalized for other applications. Applications, where the data analysis workflow is not yet clear, would benefit from considering the previous workflow approach within the design of visual analysis framework. Considerable change in the workflow, e.g. by extending the data modality, could happen in many applications, but it is especially the case for research in early stages. When searching for new things, it is often not known what might be interesting to see in the data, and the data analysis workflow might evolve over time, but visual analysis would be beneficial nonetheless. In such cases, tasks might not yet be defined at the lower domain level. Consideration of the previous research approach within the design of visual analysis framework would facilitate integration of the data legacy, users' adaptability, and tasks' consistency in the framework, thereby supporting the users in their evolving workflows.

CHAPTER 6

Conclusion and Future Work

We provided a visual analysis pipeline for comparing differences in HR and HRV during TMS. To effectively support the design of a pipeline for the visual analysis of TMS and HR data, we introduced Data–Users–Workflow-Tasks design pyramid as an extension of D-U-T triangle [Miksch and Aigner, 2014]. We proposed considering a previous research workflow approach within the design of a visual analysis pipeline by integrating data legacy, users' adaptability, and tasks compatibility. Our main focus was to support early-stage research. We enable domain experts to investigate the state dependency of HR and the impact of TMS impulses on HR and HRV. With slight changes, our visual analysis pipeline could be used for other ECG and HR comparisons. We provide an interactive pre-processing pipeline of the ECG data. We measure DTW distance between HR of two different runs of one patient and user-selected time blocks with different conditions, with focus on blocks with vs without TMS impulses. In a scatterplot, domain experts can choose the block pairs of interest to visualize the DTW distance. We compute over 80 different HRV metrics. Users can either manually choose the metrics of interest or provide a PCA to gain the metrics that most contribute to change in the HRV. These HRV metrics are visualized via clustermap that combines a heatmap with dendrogram clustering. Domain experts can choose parameters to evaluate whether time series with the same parameter were clustered together.

Future integration of fMRI presents some challenges. In our pipeline, the NCG-TMS analysis occurs over comparison of blocks or whole sessions. Even though, in the TMS-fMRI analysis it used previously to compare fMRI before and after the stimulation session, the state-of-the-art concurrent TMS-fMRI determines the immediate response. To compare the effects of TMS on fMRI with the effects of the TMS on ECG, the same periods of time would need to be considered. We did not focus on frequency analysis as was done in previous work by Dijkstra et al. [2023, 2024]. In terms of aligning time periods of TMS-fMRI and TMS-ECG analysis, including time-frequency analysis and other approaches, might be considered in the future and further investigated their

incorporation into the trimodal TMS-fMRI-ECG analysis approach. Furthermore, fMRI data are in volumetric space and would need to be transformed into feature space. We limited the noise reduction evaluation to the powerline and the baseline wander. In the future, the magnetic field gradient could be measured to determine the effects of fMRI on the signal and enable noise reduction, specifically of the possible noise induced by fMRI. In this, we thesis provided visual analysis pipeline for TMS and ECG data exploration that could be integrated in the future trimodal TMS-fMRI-ECG analysis pipeline. To design our visual analysis pipeline, we introduced D-U-W-T pyramid which indicates opportunities to integrate the previous research approach in the design of visualization analysis frameworks for early-stage research applications in the future.

Overview of Generative AI Tools Used

Grammarly and Writefull were used for spelling, grammatical, syntactical, and stylistic errors throughout the thesis to enhance the readability of the text. The German version of abstract and title is strongly based on DeepL.com (free version; September 1, 2025) translations of the English abstract and title. The DeepL translations of the abstract and title were further checked by the author assisted by dictionaries and ChatGPT (model: GPT-5 mini; September 1, 2025).

List of Figures

Acronyms

concurrent TMS-fMRI Concurrent Transcranial Magnetic Stimulation - Functional Magnetic Resonance Imaging. xi, 1, 2, 7, 9, 12, 13, 27, 32–34, 67, 71, 73

D-U-T triangle Data–Users–Tasks design triangle. xi, 2–4, 27–29, 33, 63, 65, 67, 72

D-U-W-T pyramid Data–Users–Workflow-Tasks design pyramid. xi, 5, 63, 65, 67, 68

DLPFC dorsolateral prefrontal cortex. 1, 4, 7–10, 12

DTW Dynamic Time Warping. xi, 41–43, 46, 53, 54, 56, 58, 59, 62, 63, 65, 67, 73, 74

ECG electrocardiogram. xi, 1–5, 10, 12, 13, 15, 16, 20, 27, 30–34, 36–41, 47, 49, 51–53, 60–65, 67, 68, 71–74

EEG electroencephalography. 15–18, 71

fMRI Functional Magnetic Resonance Imaging. xi, 1–3, 8, 9, 12, 32, 33, 36, 64, 67, 68, 73

HBC heart-brain coupling. 11, 18, 71

HR heart rate. xi, 1–4, 10, 11, 15–18, 30, 32, 33, 35–37, 41–43, 51–58, 62–65, 67, 71, 73, 74

HRV heart rate variability. xi, 4, 10, 11, 20–22, 41–43, 51, 52, 57, 60–65, 67, 72–74

KDE kernel density estimate. 43, 44, 54, 55, 62, 73, 74

LOCF Last Observation Carried Forward. 47, 48, 73

MAE mean absolute error. 49, 50, 73

MDD major depressive disorder. xi, 1, 7, 9, 10

MRI magnetic resonance imaging. 32, 37, 64

MSE mean squared error. 49, 50, 73

MT motor threshold. 8, 11, 31

NCG-TMS Neuro-Cardiac-Guided Transcranial Magnetic Stimulation. xiii, 1, 2, 7, 10–13, 15–19, 34, 63, 67, 71

NOCB Next Observation Carried Backward. 47, 48, 73

PCA Principal Component Analysis. 4, 21, 23, 41–43, 51, 52, 57, 60, 64, 67, 72–74

QRI Qualitative Result Inspection. xi, xiii, 4, 47, 54, 55, 57, 59, 61

RMSE root mean squared error. xi, 47, 49, 63, 73

rTMS repetitive TMS. 1, 7–10, 18, 71

sgACC subgenual cingulate cortex. 10, 12

TMS Transcranial Magnetic Stimulation. xi, xiii, 1–5, 7–16, 18, 27, 30–37, 41, 58, 63–65, 67, 68, 71–73

TRD treatment-resistant depression. 1, 7, 10

VN vagus nerve. 10

Bibliography

Alemzadeh, S., Niemann, U., Ittermann, T., Völzke, H., Schneider, D., Spiliopoulou, M., Bühler, K., and Preim, B. (2020). Visual Analysis of Missing Values in Longitudinal Cohort Study Data. *Computer Graphics Forum*, 39(1):63–75. _eprint: https://onlinelibrary.wiley.com/doi/pdf/10.1111/cgf.13662.

Ali, M., Alqahtani, A., Jones, M. W., and Xie, X. (2019). Clustering and Classification for Time Series Data in Visual Analytics: A Survey. *IEEE Access*, 7:181314–181338. Conference Name: IEEE Access.

Alsallakh, B., Bögl, M., Gschwandtner, T., Miksch, S., Esmael, B., Arnaout, A., Thonhauser, G., and Wolf-Zöllner, P. (2014). A Visual Analytics Approach to Segmenting and Labeling Multivariate Time Series Data.

Balachandran, A., Ganesan, M., and Sumesh, E. P. (2014). Daubechies algorithm for highly accurate ECG feature extraction. In *2014 International Conference on Green Computing Communication and Electrical Engineering (ICGCCEE)*, pages 1–5.

Belciug, S. (2022). A Statistical Analysis Handbook for Validating Artificial Intelligence Techniques Applied in Healthcare. In Lim, C.-P., Chen, Y.-W., Vaidya, A., Mahorkar, C., and Jain, L. C., editors, *Handbook of Artificial Intelligence in Healthcare: Vol 2: Practicalities and Prospects*, pages 61–83. Springer International Publishing, Cham.

Bernard, J., Hutter, M., Reinemuth, H., Pfeifer, H., Bors, C., and Kohlhammer, J. (2019). Visual-Interactive Preprocessing of Multivariate Time Series Data. *Computer Graphics Forum*, 38(3):401–412. _eprint: https://onlinelibrary.wiley.com/doi/pdf/10.1111/cgf.13698.

Bernard, J., Ruppert, T., Goroll, O., May, T., and Kohlhammer, J. (2012). Visual-Interactive Preprocessing of Time Series Data. volume 81. Linköping University Electronic Press.

Berndt, D. J. and Clifford, J. (1994). Using dynamic time warping to find patterns in time series. In *Proceedings of the 3rd International Conference on Knowledge Discovery and Data Mining*, AAAIWS'94, pages 359–370, Seattle, WA. AAAI Press.

Billman, G. E. (2011). Heart Rate Variability – A Historical Perspective. *Frontiers in Physiology*, 2. Publisher: Frontiers.

Bond, R. R., Finlay, D. D., Nugent, C. D., and Moore, G. (2011). A review of ECG storage formats. *International Journal of Medical Informatics*, 80(10):681–697.

Bota, P., Silva, R., Carreiras, C., Fred, A., and da Silva, H. P. (2024). BioSPPy: A Python toolbox for physiological signal processing. *SoftwareX*, 26:101712.

Brehmer, M. and Munzner, T. (2013). A Multi-Level Typology of Abstract Visualization Tasks. *IEEE Transactions on Visualization and Computer Graphics*, 19(12):2376–2385. Conference Name: IEEE Transactions on Visualization and Computer Graphics.

Buschman, H. P., Storm, C. J., Duncker, D. J., Verdouw, P. D., van der Aa, H. E., and van der Kemp, P. (2006). Heart Rate Control Via Vagus Nerve Stimulation. *Neuromodulation: Technology at the Neural Interface*, 9(3):214–220.

Chatterjee, S., Thakur, R. S., Yadav, R. N., Gupta, L., and Raghuvanshi, D. K. (2020). Review of noise removal techniques in ECG signals. *IET Signal Processing*, 14(9):569–590. _eprint: https://onlinelibrary.wiley.com/doi/pdf/10.1049/iet-spr.2020.0104.

Chen, L., Klooster, D. C. W., Tik, M., Thomas, E. H. X., Downar, J., Fitzgerald, P. B., Williams, N. R., and Baeken, C. (2023). Accelerated Repetitive Transcranial Magnetic Stimulation to Treat Major Depression: The Past, Present, and Future. *Harvard Review of Psychiatry*, 31(3):142.

Cook, K. A. and Thomas, J. J. (2005). *Illuminating the path: The research and development agenda for visual analytics*. Pacific Northwest National Lab.(PNNL), Richland, WA (United States).

D'Agostino, R. and Pearson, E. S. (1973). Tests for Departure from Normality. Empirical Results for the Distributions of b2 and b1. *Biometrika*, 60(3):613–622. Publisher: [Oxford University Press, Biometrika Trust].

Daubechies, I. (1992). *Ten Lectures on Wavelets*. SIAM. Google-Books-ID: B3C5aG4OboIC.

Dijkstra, E., van Dijk, H., Vila-Rodriguez, F., Zwienenberg, L., Rouwhorst, R., Coetzee, J. P., Blumberger, D. M., Downar, J., Williams, N., Sack, A. T., and Arns, M. (2023). Transcranial Magnetic Stimulation–Induced Heart-Brain Coupling: Implications for Site Selection and Frontal Thresholding—Preliminary Findings. *Biological Psychiatry Global Open Science*, 3(4):939–947.

Dijkstra, E. S. A., Frandsen, S. B., van Dijk, H., Duecker, F., Taylor, J. J., Sack, A. T., Arns, M., and Siddiqi, S. H. (2024). Probing prefrontal-sgACC connectivity using TMS-induced heart–brain coupling. *Nature Mental Health*, 2(7):809–817. Publisher: Nature Publishing Group.

Ding, Z., Mei, G., Cuomo, S., Li, Y., and Xu, N. (2020). Comparison of Estimating Missing Values in IoT Time Series Data Using Different Interpolation Algorithms. *International Journal of Parallel Programming*, 48(3):534–548.

Elgendi, M., Jonkman, M., and DeBoer, F. (2010). FREQUENCY BANDS EFFECTS ON QRS DETECTION:. In *Proceedings of the Third International Conference on Bio-inspired Systems and Signal Processing*, pages 428–431, Valencia, Spain. SciTePress - Science and and Technology Publications.

Emrich, J., Koka, T., Wirth, S., and Muma, M. (2023). Accelerated Sample-Accurate R-Peak Detectors Based on Visibility Graphs. In *2023 31st European Signal Processing Conference (EUSIPCO)*, pages 1090–1094. ISSN: 2076-1465.

Federico, P., Amor-Amorós, A., and Miksch, S. (2016). A Nested Workflow Model for Visual Analytics Design and Validation. In *Proceedings of the Sixth Workshop on Beyond Time and Errors on Novel Evaluation Methods for Visualization*, BELIV '16, pages 104–111, New York, NY, USA. Association for Computing Machinery.

Fox, M. D., Buckner, R. L., White, M. P., Greicius, M. D., and Pascual-Leone, A. (2012). Efficacy of Transcranial Magnetic Stimulation Targets for Depression Is Related to Intrinsic Functional Connectivity with the Subgenual Cingulate. *Biological Psychiatry*, 72(7):595–603.

Fox, M. D., Liu, H., and Pascual-Leone, A. (2013). Identification of reproducible individualized targets for treatment of depression with TMS based on intrinsic connectivity. *NeuroImage*, 66:151–160.

Frasch, M. G. (2022). Comprehensive HRV estimation pipeline in Python using Neurokit2: Application to sleep physiology. *MethodsX*, 9:101782.

Fujiwara, T., Chou, J.-K., McCullough, A. M., Ranganath, C., and Ma, K.-L. (2017). A visual analytics system for brain functional connectivity comparison across individuals, groups, and time points. In *2017 IEEE Pacific Visualization Symposium (PacificVis)*, pages 250–259. ISSN: 2165-8773.

Fujiwara, T., Shilpika, Sakamoto, N., Nonaka, J., Yamamoto, K., and Ma, K.-L. (2021). A Visual Analytics Framework for Reviewing Multivariate Time-Series Data with Dimensionality Reduction. *IEEE Transactions on Visualization and Computer Graphics*, 27(2):1601–1611. Conference Name: IEEE Transactions on Visualization and Computer Graphics.

Ganglberger, F., Swoboda, N., Frauenstein, L., Kaczanowska, J., Haubensak, W., and Bühler, K. (2019). *BrainTrawler*: A visual analytics framework for iterative exploration of heterogeneous big brain data. *Computers & Graphics*, 82:304–320.

Garcia Caballero, H. S., Corvò, A., Meulen, F. V., Fonseca, P., Overeem, S., Wijk, J. J. V., and Westenberg, M. A. (2021). PerSleep: A Visual Analytics Approach for

Performance Assessment of Sleep Staging Models. In *Eurographics Workshop on Visual Computing for Biology and Medicine*, page 11 pages. ISBN: 9783038681403 Publisher: The Eurographics Association Artwork Size: 11 pages Version Number: 123-133.

Grosshagauer, S., Woletz, M., Vasileiadi, M., Linhardt, D., Nohava, L., Schuler, A.-L., Windischberger, C., Williams, N., and Tik, M. (2024). Chronometric TMS-fMRI of personalized left dorsolateral prefrontal target reveals state-dependency of subgenual anterior cingulate cortex effects. *Molecular Psychiatry*, pages 1–11. Publisher: Nature Publishing Group.

Gschwandtner, T., Gärtner, J., Aigner, W., and Miksch, S. (2012). A Taxonomy of Dirty Time-Oriented Data. In Quirchmayr, G., Basl, J., You, I., Xu, L., and Weippl, E., editors, *Multidisciplinary Research and Practice for Information Systems*, pages 58–72, Berlin, Heidelberg. Springer.

Gurker, W. (2018). *Statistik und Wahrscheinlichkeitstheorie using R*. TU-MV Media Verlag GmbH. Accepted: 2022-07-29T08:38:48Z.

Hamilton, P. (2002). Open source ECG analysis. In *Computers in Cardiology*, pages 101–104. ISSN: 0276-6547.

Hand, D. J., Daly, F., McConway, K., Lunn, D., and Ostrowski, E. (1993). *A Handbook of Small Data Sets*. CRC Press. Google-Books-ID: m4O1DwAAQBAJ.

Iseger, T. A., Padberg, F., Kenemans, J. L., Gevirtz, R., and Arns, M. (2017). Neuro-Cardiac-Guided TMS (NCG-TMS): Probing DLPFC-sgACC-vagus nerve connectivity using heart rate – First results. *Brain Stimulation*, 10(5):1006–1008.

Iseger, T. A., Padberg, F., Kenemans, J. L., van Dijk, H., and Arns, M. (2021). Neuro-Cardiac-Guided TMS (NCG TMS): A replication and extension study. *Biological Psychology*, 162:108097.

Iseger, T. A., van Bueren, N. E. R., Kenemans, J. L., Gevirtz, R., and Arns, M. (2020). A frontal-vagal network theory for Major Depressive Disorder: Implications for optimizing neuromodulation techniques. *Brain Stimulation*, 13(1):1–9.

Isenberg, T., Isenberg, P., Chen, J., Sedlmair, M., and Möller, T. (2013). A Systematic Review on the Practice of Evaluating Visualization. *IEEE Transactions on Visualization and Computer Graphics*, 19(12):2818–2827.

Jiao, Y., Cheng, C., Jia, M., Chu, Z., Song, X., Zhang, M., Xu, H., Zeng, X., Sun, J.-B., Qin, W., and Yang, X.-J. (2024). Neuro-cardiac-guided transcranial magnetic stimulation: Unveiling the modulatory effects of low-frequency and high-frequency stimulation on heart rate. *Psychophysiology*, 61(10):e14631. _eprint: https://onlinelibrary.wiley.com/doi/pdf/10.1111/psyp.14631.

Joshi, S. L., Vatti, R. A., and Tornekar, R. V. (2013). A Survey on ECG Signal Denoising Techniques. In *2013 International Conference on Communication Systems and Network Technologies*, pages 60–64.

Jönsson, D., Bergström, A., Forsell, C., Simon, R., Engström, M., Walter, S., Ynnerman, A., and Hotz, I. (2020). VisualNeuro: A Hypothesis Formation and Reasoning Application for Multi-Variate Brain Cohort Study Data. *Computer Graphics Forum*, 39(6):392–407. _eprint: https://onlinelibrary.wiley.com/doi/pdf/10.1111/cgf.14045.

Kher, R. (2019). Signal Processing Techniques for Removing Noise from ECG Signals. *jber*.

Király, F., Löning, M., Bagnall, T., Middlehurst, M., Ray, A., Ganesh, S., Walter, M., Oastler, G., Lines, J., ViktorKaz, Heidrich, B., Mentel, L., Mishra, S., chrisholder, Bartling, D., Shakir, A., Tsaprounis, L., RNKuhns, Krishnan, J., Gilbert, C., Baichoo, M., Angelim, F., Nshuti, F. H., Akmal, H., Wu, X., alex-gregory ds, Guzal, Owoseni, T., and Rockenschaub, P. (2025). sktime/sktime: v0.38.4.

Lam, H., Bertini, E., Isenberg, P., Plaisant, C., and Carpendale, S. (2012). Empirical Studies in Information Visualization: Seven Scenarios. *IEEE Transactions on Visualization and Computer Graphics*, 18(9):1520–1536. Conference Name: IEEE Transactions on Visualization and Computer Graphics.

Laudon, M., Webster, J., Frayne, R., and Grist, T. (1998). Minimizing interference from magnetic resonance imagers during electrocardiography. *IEEE Transactions on Biomedical Engineering*, 45(2):160–164. Conference Name: IEEE Transactions on Biomedical Engineering.

Li, K., Guo, L., Faraco, C., Zhu, D., Chen, H., Yuan, Y., Lv, J., Deng, F., Jiang, X., Zhang, T., Hu, X., Zhang, D., Miller, L. S., and Liu, T. (2012). Visual analytics of brain networks. *NeuroImage*, 61(1):82–97.

Liston, C., Chen, A. C., Zebley, B. D., Drysdale, A. T., Gordon, R., Leuchter, B., Voss, H. U., Casey, B. J., Etkin, A., and Dubin, M. J. (2014). Default Mode Network Mechanisms of Transcranial Magnetic Stimulation in Depression. *Biological Psychiatry*, 76(7):517–526.

Little, R. J. A. (1988). A Test of Missing Completely at Random for Multivariate Data with Missing Values. *Journal of the American Statistical Association*, 83(404):1198–1202. Publisher: [American Statistical Association, Taylor & Francis, Ltd.].

Liu, D., Alnegheimish, S., Zytek, A., and Veeramachaneni, K. (2022). MTV: Visual Analytics for Detecting, Investigating, and Annotating Anomalies in Multivariate Time Series. *Proc. ACM Hum.-Comput. Interact.*, 6(CSCW1):103:1–103:30.

Liu, J., Pacitti, E., Valduriez, P., and Mattoso, M. (2015). A Survey of Data-Intensive Scientific Workflow Management. *Journal of Grid Computing*, 13(4):457–493.

Maaten, L. v. d. and Hinton, G. (2008). Visualizing Data using t-SNE. *Journal of Machine Learning Research*, 9(86):2579–2605.

Makovac, E., Thayer, J. F., and Ottaviani, C. (2017). A meta-analysis of non-invasive brain stimulation and autonomic functioning: Implications for brain-heart pathways to cardiovascular disease. *Neuroscience & Biobehavioral Reviews*, 74:330–341.

Makowski, D., Pham, T., Lau, Z. J., Brammer, J. C., Lespinasse, F., Pham, H., Schölzel, C., and Chen, S. H. A. (2021). NeuroKit2: A Python toolbox for neurophysiological signal processing. *Behavior Research Methods*, 53(4):1689–1696.

McConnell, K. A., Nahas, Z., Shastri, A., Lorberbaum, J. P., Kozel, F. A., Bohning, D. E., and George, M. S. (2001). The transcranial magnetic stimulation motor threshold depends on the distance from coil to underlying cortex: a replication in healthy adults comparing two methods of assessing the distance to cortex. *Biological Psychiatry*, 49(5):454–459.

McInnes, L., Healy, J., Saul, N., and Großberger, L. (2018). UMAP: Uniform Manifold Approximation and Projection. *Journal of Open Source Software*, 3(29):861.

McSharry, P. and Clifford, G. (2003). ECGSYN - A realistic ECG waveform generator v1.0.0.

McSharry, P., Clifford, G., Tarassenko, L., and Smith, L. (2003). A dynamical model for generating synthetic electrocardiogram signals. *IEEE Transactions on Biomedical Engineering*, 50(3):289–294.

Miksch, S. and Aigner, W. (2014). A matter of time: Applying a data–users–tasks design triangle to visual analytics of time-oriented data. *Computers & Graphics*, 38:286–290.

Mir, H. Y. and Singh, O. (2021). ECG denoising and feature extraction techniques – a review. *Journal of Medical Engineering & Technology*, 45(8):672–684. Publisher: Taylor & Francis _eprint: https://doi.org/10.1080/03091902.2021.1955032.

Mizutani-Tiebel, Y., Tik, M., Chang, K.-Y., Padberg, F., Soldini, A., Wilkinson, Z., Voon, C. C., Bulubas, L., Windischberger, C., and Keeser, D. (2022). Concurrent TMS-fMRI: Technical Challenges, Developments, and Overview of Previous Studies. *Frontiers in Psychiatry*, 13.

Munzner, T. (2009). A Nested Model for Visualization Design and Validation. *IEEE Transactions on Visualization and Computer Graphics*, 15(6):921–928. Conference Name: IEEE Transactions on Visualization and Computer Graphics.

Mustra, M., Delac, K., and Grgic, M. (2008). Overview of the DICOM standard. In *2008 50th International Symposium ELMAR*, volume 1, pages 39–44. ISSN: 1334-2630.

Okoye, K. and Hosseini, S. (2024). Understanding the Different Types of Statistical Data Analysis and Methods. In Okoye, K. and Hosseini, S., editors, *R Programming: Statistical Data Analysis in Research*, pages 109–127. Springer Nature, Singapore.

Oster, J., Pietquin, O., Kraemer, M., and Felblinger, J. (2010). Nonlinear Bayesian Filtering for Denoising of Electrocardiograms Acquired in a Magnetic Resonance Environment. *IEEE Transactions on Biomedical Engineering*, 57(7):1628–1638. Conference Name: IEEE Transactions on Biomedical Engineering.

O'Reardon, J. P., Solvason, H. B., Janicak, P. G., Sampson, S., Isenberg, K. E., Nahas, Z., McDonald, W. M., Avery, D., Fitzgerald, P. B., Loo, C., Demitrack, M. A., George, M. S., and Sackeim, H. A. (2007). Efficacy and Safety of Transcranial Magnetic Stimulation in the Acute Treatment of Major Depression: A Multisite Randomized Controlled Trial. *Biological Psychiatry*, 62(11):1208–1216.

Pan, J. and Tompkins, W. J. (1985). A Real-Time QRS Detection Algorithm. *IEEE Transactions on Biomedical Engineering*, BME-32(3):230–236. Conference Name: IEEE Transactions on Biomedical Engineering.

Pearson, K. (1901). LIII. On lines and planes of closest fit to systems of points in space. *The London, Edinburgh, and Dublin Philosophical Magazine and Journal of Science*, 2(11):559–572. Publisher: Taylor & Francis _eprint: https://doi.org/10.1080/14786440109462720.

Pham, T., Lau, Z. J., Chen, S. H. A., and Makowski, D. (2021). Heart Rate Variability in Psychology: A Review of HRV Indices and an Analysis Tutorial. *Sensors (Basel, Switzerland)*, 21(12):3998.

Preim, B. and Botha, C. P. (2013). *Visual computing for medicine: theory, algorithms, and applications*. Newnes.

Ratanamahatana, C. A. and Keogh, E. (2005). Three Myths about Dynamic Time Warping Data Mining. In *Proceedings of the 2005 SIAM International Conference on Data Mining (SDM)*, Proceedings, pages 506–510. Society for Industrial and Applied Mathematics.

Rossi, S., Santarnecchi, E., Valenza, G., and Ulivelli, M. (2016). The heart side of brain neuromodulation. *Philosophical Transactions of the Royal Society A: Mathematical, Physical and Engineering Sciences*, 374(2067):20150187. Publisher: Royal Society.

RUBIN, D. B. (1976). Inference and missing data. *Biometrika*, 63(3):581–592.

Rusjan, P. M., Barr, M. S., Farzan, F., Arenovich, T., Maller, J. J., Fitzgerald, P. B., and Daskalakis, Z. J. (2010). Optimal transcranial magnetic stimulation coil placement for targeting the dorsolateral prefrontal cortex using novel magnetic resonance image-guided neuronavigation. *Human Brain Mapping*, 31(11):1643–1652. _eprint: https://onlinelibrary.wiley.com/doi/pdf/10.1002/hbm.20964.

Sack, A. T., Paneva, J., Küthe, T., Dijkstra, E., Zwienenberg, L., Arns, M., and Schuhmann, T. (2023). Target Engagement and Brain State Dependence of Transcranial Magnetic Stimulation: Implications for Clinical Practice. *Biological Psychiatry*, 0(0). Publisher: Elsevier.

Salvador, S. and Chan, P. (2007). Toward accurate dynamic time warping in linear time and space. *Intelligent Data Analysis*, 11(5):561–580. Publisher: SAGE Publications.

Saritha, C., Sukanya, V., and Murthy, Y. N. (2008). ECG Signal Analysis Using Wavelet Transforms. 35:68–77.

Shaffer, F. and Ginsberg, J. P. (2017). An Overview of Heart Rate Variability Metrics and Norms. *Frontiers in Public Health*, 5:258.

Shokoohi-Yekta, M., Hu, B., Jin, H., Wang, J., and Keogh, E. (2017). Generalizing DTW to the multi-dimensional case requires an adaptive approach. *Data mining and knowledge discovery*, 31(1):1–31.

Singh, P., Srivastava, I., Singhal, A., and Gupta, A. (2019). Baseline Wander and Power-Line Interference Removal from ECG Signals Using Fourier Decomposition Method. In Tanveer, M. and Pachori, R. B., editors, *Machine Intelligence and Signal Analysis*, pages 25–36, Singapore. Springer.

Steffen, M., Sarda, A., Artz-Beielstein, T., Zaefferer, M., and Strok, J. (2015). Comparison of different methods for univariate time series imputation in R. *Cologne University of Applied Science*, pages 1–20.

Stoiber, C., Ceneda, D., Wagner, M., Schetinger, V., Gschwandtner, T., Streit, M., Miksch, S., and Aigner, W. (2022). Perspectives of visualization onboarding and guidance in VA. *Visual Informatics*, 6(1):68–83.

Tik, M., Hoffmann, A., Sladky, R., Tomova, L., Hummer, A., Navarro de Lara, L., Bukowski, H., Pripfl, J., Biswal, B., Lamm, C., and Windischberger, C. (2017). Towards understanding rTMS mechanism of action: Stimulation of the DLPFC causes network-specific increase in functional connectivity. *NeuroImage*, 162:289–296.

Tik, M., Vasileiadi, M., Woletz, M., Linhardt, D., Schuler, A.-L., Williams, N., and Windischberger, C. (2023a). Concurrent TMS/fMRI reveals individual DLPFC dose-response pattern. *NeuroImage*, 282:120394.

Tik, M., Woletz, M., Kranz, G., Pfabigan, D., Geissberger, N., Sladky, R., Kraus, C., Auer, B., Vanicek, T., Paul, K., Lanzenberger, R., Lamm, C., and Windischberger, C. (2019). Remission from depression and tms over left DLPFC share the same network connectivity changes. *Brain Stimulation: Basic, Translational, and Clinical Research in Neuromodulation*, 12(2):435–436. Publisher: Elsevier.

Tik, M., Woletz, M., Schuler, A. L., Vasileiadi, M., Cash, R. F. H., Zalesky, A., Lamm, C., and Windischberger, C. (2023b). Acute TMS/fMRI response explains offline TMS network effects – An interleaved TMS-fMRI study. *NeuroImage*, 267:119833.

Trigo, J. D., Alesanco, , Martínez, I., and García, J. (2012). A Review on Digital ECG Formats and the Relationships Between Them. *IEEE Transactions on Information Technology in Biomedicine*, 16(3):432–444.

Udupa, K., Sathyaprabha, T. N., Thirthalli, J., Kishore, K. R., Raju, T. R., and Gangadhar, B. N. (2007). Modulation of cardiac autonomic functions in patients with major depression treated with repetitive transcranial magnetic stimulation. *Journal of Affective Disorders*, 104(1):231–236.

Valero-Cabré, A., Amengual, J. L., Stengel, C., Pascual-Leone, A., and Coubard, O. A. (2017). Transcranial magnetic stimulation in basic and clinical neuroscience: A comprehensive review of fundamental principles and novel insights. *Neuroscience & Biobehavioral Reviews*, 83:381–404.

van Buuren, S. (2018). *Flexible Imputation of Missing Data, Second Edition*. CRC Press. Google-Books-ID: lzb3DwAAQBAJ.

Van Der Maaten, L., Postma, E., and Van Den Herik, J. (2009). Dimensionality Reduction: A Comparative Review. *Journal of machine learning research*, 10:66–71.

Wachowiak, M. P., Hay, D. C., and Johnson, M. J. (2015). Quantification of Wavelet Band Metrics for Assessing Heart Rate Variability. In Jaffray, D. A., editor, *World Congress on Medical Physics and Biomedical Engineering, June 7-12, 2015, Toronto, Canada*, pages 1026–1029, Cham. Springer International Publishing.

Wachowiak, M. P., Hay, D. C., Wachowiak-Smolíková, R., DuVal, D. J., and Johnson, M. J. (2016). Analyzing multiresolution wavelet entropy of ECG with visual analytics techniques. In *2016 IEEE Canadian Conference on Electrical and Computer Engineering (CCECE)*, pages 1–5.

wannesm, khendrickx, Yurtman, A., Robberechts, P., Vohl, D., Ma, E., Verbruggen, G., Rossi, M., Shaikh, M., Yasirroni, M., Todd, Zieliński, W., Craenendonck, T. V., and Wu, S. (2022). wannesm/dtaidistance: v2.3.5.

Ward, H. B., Brady, R. O. J., and Halko, M. A. (2021). Bridging the Gap: Strategies to Make Psychiatric Neuroimaging Clinically Relevant. *Harvard Review of Psychiatry*, 29(3):185.